Journal of Neuroinflammation

RESEARCH | Article in Press

FAM84B promotes intercellular tau transfer through exocytic tau export in response to neuroinflammatory signaling

Gwangho Yoon · Hyeyeon Park · Jee-Yun Park · Min Kyoung Kam · Jung-Hyun Kim · Eun-Joo Kim · Sung-Hye Park · Hyunyoung Kim · Gail VW Johnson · Ji-Young Choi · Young Ho Koh · Chulman Jo

Received: 12 May 2026 / Accepted: 26 September 2026
© The Author(s) 2026

Abstract

Background The increasing prevalence of dementia underscores the pressing need for effective therapeutic interventions. Despite extensive research into amyloid-β, the modest clinical benefits achieved to date have prompted growing interest in tau pathology and intercellular tau transfer as potential therapeutic targets. However, molecular regulators linking neuroinflammation to tau transfer remain poorly understood.

Main body Here, we identified family with sequence similarity 84 member B (FAM84B; also known as LRATD2) as a novel regulator of intercellular tau transfer. Elevated FAM84B levels were detected in postmortem cortical tissues from patients with tauopathies and induced pluripotent stem cell-derived cortical neurons from patients with AD. Increased FAM84B expression enhanced tau secretion in association with ryanodine receptor 3-linked calcium signaling, and the released tau was subsequently taken up by neighboring cells in part through clathrin-associated endocytosis, thereby promoting cell-to-cell tau transfer. We further found that neuroinflammatory signaling involving signal transducer and activator of transcription 3 activation was associated with increased tau transfer. Proinflammatory cytokine treatment upregulated FAM84B expression, whereas pharmacological inhibition of ryanodine receptor signaling with dantrolene, suppressed the associated increase in tau transfer.

Conclusion FAM84B may participate in a neuroinflammation-associated process that redistributes tau toward extracellular release and intercellular transfer. These findings identify a potential mechanistic link between neuroinflammation and tau transfer and highlight FAM84B-associated pathways as potential mechanistic targets for further investigation in tauopathies.

Keywords Alzheimer's disease · Extracellular vesicles · FAM84B · Neuroinflammation · Ryanodine receptor 3 · Tau transfer

This Article in Press is shared early to give you faster access to new research. It is citable and carries a permanent DOI. The final edited version will replace it automatically.

Gwangho Yoon and Hyeyeon Park equally contributed to this work.



https://doi.org/10.1186/s12974-026-04069-7

Published online: 02 October 2026

Abbreviations

AAV	Adeno-associated virus
AD	Alzheimer's disease
BDNF	Brain-derived neurotrophic factor
BSA	Bovine serum albumin
CBD	Corticobasal degeneration
CHC	Clathrin heavy chain
CME	Clathrin-mediated endocytosis
CM	Conditioned medium
CN	Cortical neuron
CNS	Central nervous system
CSF	Cerebrospinal fluid
DAPI	4′,6-diamidino-2-phenylindole
DEG	Differentially expressed gene
DMEM	Dulbecco's modified Eagle medium
DMSO	Dimethyl sulfoxide
DNase	Deoxyribonuclease
EB	Embryoid body
ECL	Enhanced chemiluminescence
EDTA	Ethylenediaminetetraacetic acid
EGF	Epidermal growth factor
ELISA	Enzyme-linked immunosorbent assay
EV	Extracellular vesicle
FAM84B	Family with sequence similarity 84 member B
FBS	Fetal bovine serum
FGF-2	Fibroblast growth factor 2
FTD	Frontotemporal dementia
GFP	Green fluorescent protein
GO	Gene ontology
gRNA	Guide RNA
HC	Healthy control
HEK293	Human embryonic kidney 293
iPSC	Human induced pluripotent stem cell
HRP	Horseradish peroxidase
IL-6	Interleukin-6
KO	Knockout
LAMP	Lysosome-associated membrane protein
LC3	Microtubule-associated protein 1 light chain 3
LRATD2	Lecithin retinol acyltransferase domain containing 2
MAPT	Microtubule-associated protein tau
MCI	Mild cognitive impairment
MISEV	Minimal Information for Studies of Extracellular Vesicles
mRNA	Messenger RNA
NT-3	Neurotrophin-3
OCT	Optimal cutting temperature compound
OE	Overexpression
PART	Primary age-related tauopathy

PBS	Phosphate-buffered saline
PHF-1	Phosphorylated tau at residues S396/S404
PSP	Progressive supranuclear palsy
PVDF	Polyvinylidene difluoride
RIPA	Radioimmunoprecipitation assay
RNA-seq	RNA sequencing
RYR3	Ryanodine receptor 3
SDS-PAGE	Sodium dodecyl sulfate-polyacrylamide gel electrophoresis
SEM	Standard error of the mean
SH-SY5Y	Human neuroblastoma SH-SY5Y cell line
STAT3	Signal transducer and activator of transcription 3
TNF-α	Tumor necrosis factor-alpha
VD	Vascular dementia
WB	Western blot
WT	Wild type

Introduction

The rising prevalence of dementia and persistent challenges in developing effective treatments underscore the urgent need for a deeper understanding of disease mechanisms and therapeutically actionable targets [1]. Despite extensive efforts to target Aβ in Alzheimer's disease (AD), the clinical benefits achieved to date have remained modest [2, 3]. These outcomes highlight the complexity of AD pathophysiology and the need to investigate complementary disease mechanisms and therapeutic targets [4].

Accordingly, tau pathology has emerged as an important focus of dementia research. Aberrant modifications of the tau protein, including hyperphosphorylation and aggregation, are observed in various neurodegenerative disorders, but the biochemical composition and neuropathological distribution of tau pathology differ substantially among diseases [5]. AD is characterized by mixed 3-repeat (3R) and 4-repeat (4R) tau aggregates together with Aβ amyloid pathology [5] and is frequently accompanied by additional age-related co-pathologies, including α-synuclein pathology [6]. In contrast, progressive supranuclear palsy (PSP) and corticobasal degeneration (CBD) are predominantly 4R tauopathies, with PSP typically characterized by tufted astrocytes and oligodendroglial coiled bodies, whereas CBD exhibits astrocytic plaques and coiled bodies [7]. Primary age-related tauopathy (PART) is characterized by AD-type 3R+4R neurofibrillary tau pathology occurring in the absence of substantial Aβ deposition [8]. These distinct pathological backgrounds provide a framework for considering whether molecular alterations associated with tau pathology are related to a particular tau isoform class or are shared across different tauopathies. To distinguish molecular changes associated with tauopathies from those accompanying dementia with a primarily vascular etiology, vascular dementia (VD) is included as a disease comparator. VD is primarily associated with cerebrovascular injury rather than being classified as a primary tauopathy [9]. However, because incidental AD-related tau and Aβ pathologies can occur in individuals with VD, this group was considered a non-primary tauopathy comparator rather than an unequivocally tau-negative control [10]. Tau-directed strategies, including inhibition of tau aggregation, enhancement of tau clearance, and modulation of tau-related cellular pathways, remain under active investigation, but effective treatments have yet to be established [11–15].

Intercellular tau transfer has emerged as an important focus in neurodegeneration research [16]. Proposed routes include activity-dependent tau release, EV-associated secretion, transfer through tunneling nanotubes, and receptor-mediated endocytosis [17–19]. Although strategies to inhibit intracellular tau aggregation and intercellular spread are being pursued, the molecular regulators governing tau export and recipient-cell uptake remain incompletely defined [20, 21]. Neuroinflammatory signaling is increasingly recognized as an important

component of neurodegenerative disease and may influence tau homeostasis, release, and intercellular transfer [7, 22]. However, the molecular mechanisms connecting inflammatory signaling to tau release and intercellular transfer remain incompletely understood. Identifying factors that bridge these processes may therefore provide insight into how inflammatory environments influence tau redistribution.

In the present study, we identified FAM84B, also known as LRATD2, as a regulator of intercellular tau transfer linked to neuroinflammation. By examining FAM84B across neuropathologically distinct tauopathies and a non-primary tauopathy disease comparator, we explored whether FAM84B alterations were observed across distinct tauopathy backgrounds without inferring direct tau isoform specificity. Our findings suggest that FAM84B may participate in a neuroinflammation-associated process that redistributes tau from intracellular stores toward extracellular release and intercellular transfer.

Materials and methods

Ethics statement

Participants were identified from the Seoul National University Hospital Brain Bank (SNUHBB) and Pusan National University Hospital Brain Bank (PNUHBB), and written informed consent was obtained from each patient or their legal guardian prior to death. This study adhered to the guidelines approved by the Institutional Review Board of the Korea Disease Control and Prevention Agency (KDCA; IRB number: 2022-07-06-2C-A), which governs the use of human brain tissue and cerebrospinal fluids. All experimental procedures were conducted in accordance with established ethical standards and guidelines. This research was conducted in compliance with the Declaration of Helsinki and the ethical principles outlined by the KDCA. Additionally, the confidentiality and anonymity of participants were maintained throughout the study. The data used in this study were anonymized prior to analysis to maintain the privacy of the participants.

Human brain tissue

Postmortem cerebral cortical tissues were obtained from SNUHBB and PNUHBB, where postmortem neuropathological examinations were conducted. Samples were obtained from the entorhinal cortex and middle temporal gyrus, with the region analyzed for each donor indicated in Supplementary Table 1A. Diagnoses of VD, CBD, PSP, PART, and AD were made according to the criteria stipulated by the National Institute on Aging and Alzheimer's Association guidelines (NIA-AA). Brain tissues were collected following standard protocols and immediately frozen at −80°C for storage prior to analysis.

Detailed clinical and neuropathological information for each postmortem donor, including age at death, sex, postmortem interval (PMI), APOE genotype, Braak neurofibrillary tangle stage, CERAD neuritic plaque score, Aβ pathology, and relevant co-pathologies, was obtained from the respective brain banks and is summarized in Supplementary Table 1A.

The postmortem samples analyzed for FAM84B, CHC, and phosphorylated STAT3 in Figs. 1A, 4B, and 5C, respectively, were derived from this donor cohort, with the individual samples included in each analysis indicated in Supplementary Table 1A.

Human cerebrospinal fluid

The human CSF used in this study was obtained from PNUHBB. Prior to inclusion, each participant provided informed consent in accordance with established guidelines and regulations. A neurologist specializing in neurodegenerative diseases conducted comprehensive evaluations, including clinical interviews and neurological examinations. Mild cognitive impairment and AD were diagnosed according to the modified Petersen criteria and

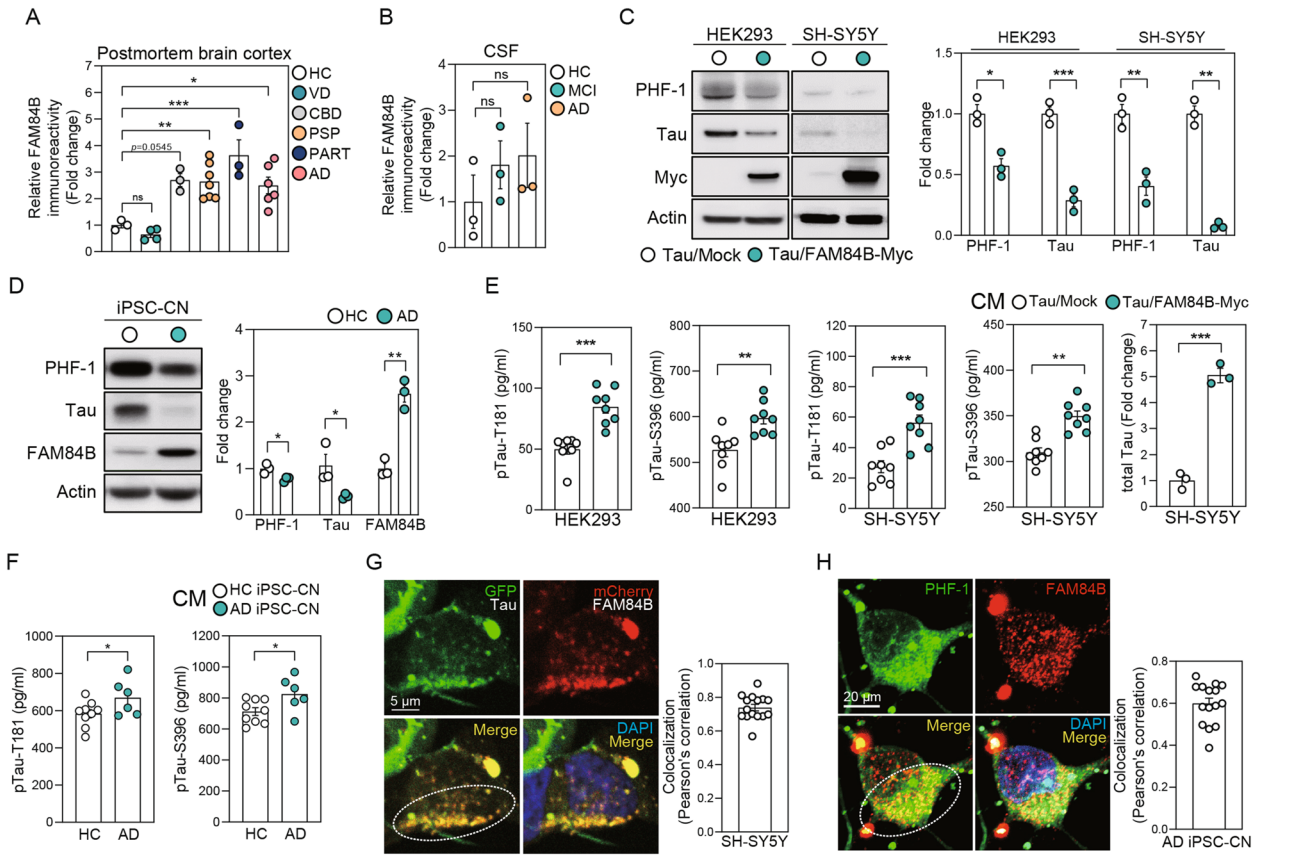


Fig. 1 FAM84B promotes extracellular release of phosphorylated and total tau. **A** FAM84B levels in the cerebral cortex of HC (n=3) and patients with VD (n=4), CBD (n=3), PSP (n=7), PART (n=3), and AD (n=6). **B** Relative FAM84B immunoreactivity in the CSF of HC and patients with MCI and AD (n=3 each). **C** Levels of PHF-1, total tau, and FAM84B-Myc in HEK293 and SH-SY5Y cells expressing human 2N4R tau alone or 2N4R tau together with FAM84B-Myc (n=3 each). **D** Levels of PHF-1, total tau, and FAM84B in iPSC-derived CN from the HC and AD groups (n=3 each). Both HC and AD groups represent pooled samples generated by physically combining equal amounts of material from the two respective iPSC lines for each independent experiment. **E** Levels of phosphorylated tau (T181 and S396; n=8 each) and total tau (n=3 each) in the CM from HEK293 and SH-SY5Y cells expressing tau alone or tau with FAM84B-Myc. **F** Levels of phosphorylated tau (T181 and S396) in the CM from pooled HC and AD iPSC-derived CN samples (HC, n=9; AD, n=6). Each independent sample was generated by physically pooling equal amounts of material from the two respective iPSC lines. **G** Colocalization (dashed circle) of tau and FAM84B in SH-SY5Y cells expressing GFP-tau and mCherry-FAM84B (n=15). **H** Colocalization (dashed circle) of tau and FAM84B in pooled AD iPSC-derived CN cultures generated from the two AD iPSC lines (n=15 fields). Results are presented as mean ± SEM. Colocalization analysis: (**G**, **H**) Pearson's correlation coefficient. Statistical analyses: (**A**) ordinary one-way ANOVA followed by Tukey's multiple-comparisons test; (**B**) ordinary one-way ANOVA followed by Dunnett's post hoc test; (**C**–**F**) unpaired two-tailed t-test with Welch's correction; ns: not significant, *$p < 0.05$, **$p < 0.01$, and ***$p < 0.001$. Abbreviations: HC, healthy controls; VD, vascular dementia; CBD, corticobasal degeneration; PSP, progressive supranuclear palsy; PART, primary age-related tauopathy; AD, Alzheimer's disease; CSF, cerebrospinal fluid; MCI, mild cognitive impairment; CN, cortical neurons; CM, conditioned medium; PHF-1, phosphorylated tau at residues S396/S404

the NIA-AA core clinical criteria, respectively. CSF collection, involving nine subjects, adhered to established protocols and was conducted at the Research Institute for Convergence of Biomedical Science and Technology at the Pusan National University Yangsan Hospital. CSF samples were immediately frozen and stored at −80°C prior to analysis. Equal volumes of CSF were subjected to immunoblot analysis, and FAM84B band intensities were normalized to total lane protein determined by Ponceau S staining. Demographic information for the CSF participants, including age and sex, is provided in Supplementary Table 1B.

Cell lines and culture

Mouse Neuro-2A, human HEK293, and SH-SY5Y neuroblastoma cells were obtained from the American Type Culture Collection (ATCC). Neuro-2A and HEK293 cells were cultured in Dulbecco's Modified Eagle medium (DMEM; Thermo Fisher Scientific, Waltham, MA, USA) supplemented with 10% fetal bovine serum (FBS; Merck Millipore, Burlington, MA, USA), 1 mM sodium pyruvate (Thermo Fisher Scientific), and 100 U/ml penicillin-streptomycin (Thermo Fisher Scientific). SH-SY5Y cells were cultured in DMEM/F12 containing 10% FBS and 100 U/ml penicillin-streptomycin. All cells were maintained at 37 °C in a 5% CO_2 atmosphere, and the medium was refreshed every two days. Sub-culturing was performed using prewarmed 1× PBS (Thermo Fisher Scientific) and 0.25% trypsin-EDTA (Thermo Fisher Scientific).

Neuronal differentiation of Neuro-2A and SH-SY5Y cells was initiated by supplementing the DMEM/F12 medium with 10 µM all-trans retinoic acid (Sigma-Aldrich, Burlington, MA, USA), 2% FBS, and 100 U/ml penicillin-streptomycin. The medium was renewed every two days until the cells reached a differentiated state by day 5.

Human induced pluripotent stem cell (iPSC) was cultured on vitronectin-coated plates (Gibco, Thermo Fisher Scientific) in TeSR-E8 medium (Stem Cell Technologies, Vancouver, CA). The culture medium was replaced daily. For subculturing, the cells were dissociated using EDTA (Gibco). The normal iPSC lines hFSiPS3-1 and PB01-EiPS21 were procured from the Korea National Stem Cell Bank. The AD iPSC lines UCSD234i-SAD2-3 (sporadic AD) and UCSD241i-APP2-3 (APP-associated familial AD) were obtained from WiCell Research Institute Inc (Madison, WI, USA) [23, 24].

The two control iPSC lines (hFSiPS3-1 and PB01-EiPS21) and the two AD iPSC lines (UCSD234i-SAD2-3 and UCSD241i-APP2-3) were used to generate diagnostic-group samples. For each independent experiment, equal amounts of material from the two iPSC lines within each diagnostic group were physically combined to generate a single pooled sample before analysis. This pooling strategy was applied to western blot, conditioned medium, and imaging experiments. Accordingly, each *n* represents an independently generated pooled sample derived from two iPSC lines rather than an individual iPSC line.

iPSC-derived cortical neurons and brain organoids

Differentiation of iPSC-derived cortical neurons and brain organoids was performed as previously described, with some modifications [25]. Briefly, iPSCs were dissociated using Accutase® solution (Sigma-Aldrich). A total of 9,000 cells per well were cultured in AggreWell™ EB formation medium (Stem Cell Technologies) with 1× CloneR™ (Stem Cell Technologies) in Ultra Low Cluster 96-well plates (Costar, Corning, NY, USA). On day 2, the formed embryoid bodies (EBs) were transferred to a petri dish (SPL) and cultured in AggreWell™ EB formation medium supplemented with 2.5 µM Dorsomorphin dihydrochloride (Tocris Bioscience, Bristol, UK) and 10 µM SB431542 (Tocris), with daily medium changes. On day 7, EBs were cultured in neurobasal medium (Gibco) supplemented with 2% B-27 without vitamin A (Gibco), 1% GlutaMax (Gibco), 20 ng/ml EGF (R&D Systems, Minneapolis, MN, USA), and 20 ng/ml FGF-2 (PeproTech, Cranbury, NJ, USA), with daily medium changes.

On days 21–23, for cortical neuron differentiation, EBs were dissociated using 0.05% Trypsin-EDTA (Gibco) and plated on dishes coated with 50 µg/ml Poly-L-ornithine (Sigma-Aldrich) and 20 µg/ml Laminin (Sigma-Aldrich). Cells were cultured in DMEM/F12 medium (Gibco) supplemented with antibiotic-antimycotic (Gibco), 2% B-27 without vitamin A (Gibco), 1% N-2 (Gibco), 20 ng/ml brain-derived neurotrophic factor (BDNF; R&D Systems), and 20 ng/ml NT-3 (R&D Systems). The medium was changed every other day. On day 25, for brain organoid differentiation, EBs were cultured in neurobasal medium (Gibco) supplemented with 2% B-27 without vitamin A (Gibco), 1% GlutaMax (Gibco), 20 ng/ml BDNF (R&D Systems), and 20 ng/ml NT-3 (R&D Systems). The medium was changed every other day. Cortical neurons and brain organoids were cultured for at least 40 days.

Generation of stable cell lines

To establish stable tau-expressing cell lines, HEK293 cells were transfected with pcDNA3.1-Tau(2N4R), which carries a neomycin resistance gene, using Lipofectamine 3000 (Thermo Fisher Scientific). Following a 48-hour post-transfection period, neomycin selection was initiated with G418 (Gibco) at doses determined via a kill curve (1–5 μg/ml). Multiple G418-resistant colonies were isolated using cloning rings and screened for tau expression by western blotting. For the initial microarray-based discovery analysis, one clone with relatively high intracellular tau levels was compared with one clone with relatively low tau levels.

To generate stable FAM84B knockout cell lines, we used the FAM84B human gene knockout kit (OriGene, Rockville, MD, USA) following the manufacturer's protocol. HEK293 cells were transfected with FAM84B gRNA vectors (or scrambled controls) and linear donor DNA (LoxP-EF1A-tGFP-P2A-Puro-LoxP) using Lipofectamine 3000 (Thermo Fisher Scientific). After 48 hours post-transfection, cells were passaged and cultured for 3 days, with subsequent passages every 3 days for a total of seven passages. Puromycin (Invitrogen, Thermo Fisher Scientific) selection was initiated at the 5^{th} or 7^{th} passage, with doses determined via a kill curve (1–10 μg/ml). Puromycin-resistant cells and individual cell colonies were isolated using cloning rings and analyzed by western blotting and genomic PCR to confirm donor-cassette integration and loss of FAM84B protein expression.

Plasmid construction and subcloning

A combination of plasmids was used to elucidate the role of FAM84B in tauopathy. These included: pcDNA3.1-Tau(2N4R) (Gail VW Johnson Lab), pCMV6-FAM84B-Myc-DDK (OriGene #RC207996), pEGFP-C1-Tau(2N4R) (Gail VW Johnson Lab), pmCherry-C1-FAM84B (subcloning using *KpnI*/*EcoRI*), pcDNA3.1-Tau(2N4R)-p2a-eGFP (subcloning using *BamHI*/*XhoI*), pcDNA3.1-Tau(2N4R) (P301L)-VC (Addgene #87633), pcDNA3.1-VN-Tau(2N4R) (P301L) (Addgene #87634), pcDNA3.1-STAT3-WT (JE Darnell Jr Lab), and pcDNA3.1-STAT3-DN (JE Darnell Jr Lab). All subcloned plasmids were confirmed by sequencing and protein expression analysis and were used for transient transfection. The primer sequences used are listed in Supplementary Table 2.

Additionally, we used plasmids from the AAVpro Helper Free Systems (Takara Bio, Kusatsu, Japan) to investigate the role of FAM84B in iPSC-derived cortical neurons and brain organoids. These included: pAAV-FAM84B (subcloning using *EcoRI*/*BamHI*), pAAV-FAM84B-Myc (subcloning using *EcoRI*/*BamHI*), and pAAV-Tau(2N4R)-Myc-p2a-eGFP (subcloning using *EcoRI*/*XbaI*). All plasmids were confirmed by sequencing and used for AAV infection. The primer sequences used are listed in Supplementary Table 2.

For additional protein cargo analyses, plasmids encoding human APP carrying the Swedish mutation (APPsw), α-synuclein-Myc, and GFP were also used. pcDNA3.1-APPsw, pcDNA3.1-α-synuclein-Myc, and pEGFP-C1 were used for transient transfection as indicated.

Preparation of AAV particles

AAV6 particles were produced by co-transfecting HEK293T cells (ATCC) with a triple plasmid system [pAAV, pRC6, and pHelper] provided by the AAVpro Helper Free system (Takara Bio). After 72 h, AAV particles were harvested from the transfected cells using an AAVpro purification kit (Takara Bio). Recombinant AAV-mediated expression of the proteins of interest was confirmed by western blot analysis.

Transfection and treatment

Human HEK293 and SH-SY5Y cells were transfected with pcDNA3.1-Tau(2N4R), pcDNA3.1-Tau(2N4R) (P301L)-VC, pcDNA3.1-VN-Tau(2N4R) (P301L), pCMV6-FAM84B-myc-DDK, pcDNA3.1-STAT3-WT, or pcDNA3.1-STAT3-DN using Lipofectamine 3000 (Thermo Fisher Scientific) following the manufacturer's protocol. All analyses were conducted at 48 h post-transfection.

For assessing neuroinflammation-mediated FAM84B expression, human SH-SY5Y cells and iPSC-derived cortical neurons were treated with sterilized distilled water (control vehicle), 50 ng/ml IL-6, or 50 ng/ml TNF-α, either separately or in combination. Analyses were performed at 48 h post-treatment.

To pharmacologically inhibit ryanodine receptor-linked cytosolic calcium regulation, human HEK293 and SH-SY5Y cells, along with iPSC-derived cortical neurons, were treated with DMSO (control vehicle) or 10 μM dantrolene (R&D Systems). All analyses were conducted at 24 h post-treatment.

To pharmacologically examine the contribution of endocytic pathways to FAM84B-associated tau uptake, human SH-SY5Y cells were treated with DMSO (control vehicle) or 10 μM Pitstop2 (Sigma-Aldrich). Analyses were performed at 24 h post-treatment.

For RYR3 knockdown experiments, SH-SY5Y cells were transfected with control siRNA (siCtr; Bioneer, SN-1001) or RYR3-targeting siRNA (siRYR3; Bioneer, 6263-1) at 10 nM using Lipofectamine 3000. Cells were subsequently subjected to the Tau-p2a-eGFP/FAM84B-Myc tau-transfer assay. Knockdown efficiency was confirmed by western blot analysis, and Fluo-4 AM-based calcium imaging and tau-transfer analyses were performed as described below.

For CHC knockdown experiments, SH-SY5Y cells were transfected with control siRNA (siCtr; Bioneer, SN-1001) or clathrin heavy chain-targeting siRNA (siCHC; Bioneer, 1213-1) at 10 nM using Lipofectamine 3000 and subjected to the Tau-p2a-eGFP/FAM84B-Myc tau-transfer assay. CHC knockdown efficiency was confirmed by western blot analysis, and tau transfer was quantified as described below.

For additional protein cargo analyses, HEK293 cells were transfected with α-synuclein-Myc or GFP together with either control vector or FAM84B-Myc. For amyloid-β analyses, HEK293 cells were transiently transfected with APPsw together with either control vector or FAM84B-Myc. Cellular proteins and conditioned media were collected for subsequent immunoblot or ELISA analyses.

Tau transfer analyses

Two complementary donor-recipient tau transfer assays were employed to validate FAM84B-associated tau transfer.

To visualize tau transfer upon exposure to conditioned media, donor HEK293 and SH-SY5Y cells were left untransfected (Normal) or transfected with pcDNA3.1-Tau(2N4R) together with either control vector (Tau/Mock) or pCMV6-FAM84B-Myc (Tau/FAM84B-Myc) for 48 h. Conditioned media collected from each donor condition were subsequently transferred to naïve HEK293 or SH-SY5Y recipient cells for an additional 24 h before analysis.

To visualize cell-to-cell tau transfer, HEK293 and SH-SY5Y cells were transfected with pcDNA3.1-Tau(2N4R)-p2a-eGFP together with either control vector (Tau-p2a-eGFP/Mock) or pCMV6-FAM84B-Myc (Tau-p2a-eGFP/FAM84B-Myc) for 48 h.

For tau transfer analyses in iPSC-derived cortical neurons and brain organoids, cells or organoids were co-infected with AAV6-Tau(2N4R)-Myc-p2a-eGFP together with either control AAV or AAV6-FAM84B-Myc. AAV particles were maintained in the culture medium for 4 days, and the cultures were analyzed 6 days after the initiation of infection.

Tau transfer was quantified as the number of recipient cells (GFP-negative/PHF-1-positive) per field of view. GFP-positive donor cells were quantified separately to confirm comparable donor-cell numbers between experimental groups.

cDNA microarray

Total RNA was extracted from cells expressing either relatively low or high levels of tau protein using TRIzol reagent (Invitrogen) according to the manufacturer's protocol. The RNA purity and integrity were assessed using an ND-1000 Spectrophotometer (NanoDrop Technologies, Wilmington, DE, USA) and an Agilent 2100

Bioanalyzer (Agilent Technologies, Inc., Santa Clara, CA, USA). Total RNA was amplified and purified using the TargetAmp-Nano Labeling Kit for Illumina Expression BeadChip (EPICENTRE; Illumina Inc., San Diego, CA, USA) to generate biotinylated cRNA according to the manufacturer's instructions.

Briefly, 500 ng of total RNA was reverse-transcribed into cDNA using T7 oligo(dT) primers. The subsequent steps included second-strand cDNA synthesis, in vitro transcription, and biotin-NTP labeling. After purification, the cRNA was quantified using an ND-1000 Spectrophotometer. Each 750 ng of labeled cRNA sample was hybridized to a Human HT-12 v4.0 Expression BeadChip for 17 h at 58 °C, following Illumina's instructions. Array signal detection was performed using Amersham Fluorolink Streptavidin-Cy3 (GE Healthcare Bio-Sciences, Piscataway, NJ, USA) according to the bead array manual, and the arrays were scanned using an Illumina BeadArray Reader confocal scanner.

Quality control checks were performed visually on the internal controls and raw scanned data. Raw data were extracted using Illumina GenomeStudio v2011.1 software (Gene Expression Module v1.9.0), followed by logarithmic transformation and quantile normalization of the array probes. The statistical significance of the expression data was assessed using the LPE test and fold change analysis, with the false discovery rate (FDR) controlled via the adjustment of *p*-values using the Benjamini-Hochberg algorithm. Hierarchical cluster analysis of differentially expressed gene sets was conducted using complete linkage and Euclidean distance as similarity measures.

mRNA sequencing

Total RNA was extracted from the negative control, FAM84B knockout, FAM84B overexpression, and Tau/FAM84B co-overexpressing HEK293 and SH-SY5Y cells using TRIzol Reagent (Thermo Fisher Scientific), according to the manufacturer's instructions. DNase I (Takara Bio) was added and incubated for one hour to remove any residual DNA. The RNA concentration was quantified using an ND-1000 spectrophotometer (Thermo Fisher Scientific), and RNA integrity was assessed using a 2100 Expert Bioanalyzer (Agilent Technologies, Inc.).

rRNA was depleted using a Ribo-Zero Gold rRNA Removal Kit (Illumina, Inc.). Following rRNA depletion, RNA-sequencing libraries were prepared using the TruSeq Stranded mRNA Kit (Illumina, Inc.) and sequenced on a NovaSeq 6000 (Illumina, Inc.) with 2×100 bp paired-end reads.

RNA-Seq data analysis involved mapping the reads to the reference genome (human hg19) using Tophat (v2.0.13), followed by differential expression analysis using Cuffdiff (v2.2.0). Library normalization and dispersion estimation were performed using geometric and pooled methods depending on the availability of replicates. CummeRbund (v2.8.2) was used for data visualization. DEGs were identified from the "gene_exp.diff" output of Cuffdiff, filtering for genes with a "OK" status and a fold change exceeding 2.

Bioinformatic analyses

For the gene ontology (GO) analysis of the selected genes from the mRNA-seq data, we utilized the Gene Ontology Resource (http://geneontology.org/). Altered genes were analyzed by selecting their "Cellular compartment" terms. The PANTHER classification system and Fisher's exact test were employed, followed by the calculation of the false discovery rate (FDR) and fold enrichment. The selected genes and GO terms utilized are listed in Supplementary Table 3.

To predict the transcription factors and chromatin regulators involved in FAM84B expression, we used the ChIP-seq database (https://maayanlab.cloud/Harmonizome/), which includes the ENCODE and ChEA systems. This list is included in Supplementary Table 3.

To ascertain the binding regions of the predicted transcription factors to the FAM84B promoter, genomic information was sourced from the human genome (GRCh37/hg19) available on the UCSC Genome Browser (https://genome.ucsc.edu/). We then accessed public data from ENCODE ChIP-seq, GeneHancer regulatory elements and genes, and the FANTOM5 enhancer in the UCSC Genome Browser. We aligned and displayed the predicted transcription factors bound to the enhancer regions of FAM84B.

Isolation and characterization of extracellular vesicle-enriched fractions

The membrane affinity-based EV isolation process began with filtering the conditioned media through a 0.45 µm syringe filter (Pall Corporation, New York, NY, USA). The filtered media were then mixed with a binding buffer (buffer XBP) and loaded onto the membrane spin column of the ExoEasy Maxi Kit (Qiagen, Venlo, the Netherlands). After centrifugation at 500×g for 3 min, vesicles were captured within the membrane, whereas excess fluid and proteins were removed. The bound vesicle fraction was purified by adding washing buffer (buffer XWP) to the membrane, followed by centrifugation at 5,000×g for 5 min.

After replacing the collection tube, the elution buffer (buffer XE) was added to the column and incubated for 1 min at room temperature. Centrifugation at 500×g for 5 min facilitated the elution of the EV-enriched fraction. To enhance EV recovery, the eluate was reapplied to the column, incubated for 1 min at room temperature, and centrifuged at 5,000×g for 5 min. Finally, the EV-enriched fraction was collected in a final volume of 200 µl of the provided elution buffer. The isolated fractions were further characterized by immunoblotting for the EV-associated proteins Alix, TSG101, CD9, CD63, and CD81, with calnexin examined as a non-EV cellular contamination marker.

Total membrane isolation

The total membrane fraction was isolated using a Plasma Membrane Protein Extraction Kit (Abcam, Cambridge, UK). Initially, the cells were harvested by centrifugation at 600×g for 5 min, washed with ice-cold 1× phosphate-buffered saline (PBS), and suspended in the homogenization buffer mix provided by the kit. After homogenization, the resulting homogenate was centrifuged at 700×g for 10 min to remove cellular debris, and the supernatant was collected to isolate total cellular membrane proteins. After centrifugation at 10,000×g for 30 min, the cytosolic fraction remaining in the supernatant was separated from the total membrane fraction contained within the pellet.

Calcium staining

Intracellular calcium-associated fluorescence in HEK293 and SH-SY5Y cells was assessed using Fluo-4 AM solution (Invitrogen) according to the manufacturer's protocol. A 3 mM Fluo-4 AM/DMSO stock solution was diluted to a 3 µM working solution in the respective culture medium. Cells were incubated with the Fluo-4 AM working solution for 20 minutes at 37 °C in a CO_2 incubator. After incubation, the cells were washed with indicator-free medium to remove non-specifically associated dyes and then incubated with indicator-free medium for an additional 30 min to ensure complete de-esterification of intracellular AM esters. Calcium imaging and cellular morphology analyses were performed using the EVOS M5000 Imaging System (Invitrogen).

Western blot analysis

Western blot analysis was performed according to established protocols. Cells and tissues were lysed in ice-cold RIPA buffer (GenDEPOT, Altair, TX, USA) for 10 min on ice, and protein concentrations were determined using a BCA assay kit (Thermo Fisher Scientific) following the manufacturer's instructions. Protein samples (15–25 µg) were separated on 8–12% pre-made SDS-polyacrylamide gels (Thermo Fisher Scientific) and transferred onto polyvinylidene difluoride (Merck Millipore) membranes using absolute methanol (Thermo Fisher Scientific).

The membranes were blocked in a solution containing 5% bovine serum albumin (GenDEPOT) and skim milk (Cell Signaling Technology, Danvers, MA, USA) for one hour at room temperature to enhance the detection of the phosphorylated and native forms of the proteins. Following blocking, membranes were incubated overnight at 4 °C with primary antibodies (1:1,000 dilution), including: PHF-1 (Peter Davies Lab), Tau5 (Gail VW Johnson Lab), Tau (Dako, Agilent Technologies, Inc., A0024), Tau (CST, Cell signaling Technology, 30328),

6E10 (Covance, SIG-39300), GFP (Roche, 27575600), Myc-tag (Cell Signaling Technology, 2276), FAM84B (OriGene, TA501992; Proteintech Group, Inc., Rosemont, IL, USA, 18421-1-AP), Alix (Cell Signaling Technology, 2171), TSG101 (Cell Signaling Technology, 72312), CD9 (Cell Signaling Technology,13174), CD63 (Cell Signaling Technology, 52090), CD81 (Cell Signaling Technology, 56039), calnexin (Cell Signaling Technology, 2679), Caveolin-1 (Cell Signaling Technology, 3267), RYR3 (Alomone Labs, Jerusalem, Israel, ARR003), Clathrin-heavy chain (CHC, Cell Signaling Technology, 4796), EEA1 (Cell Signaling Technology, 3288), Rab5 (Cell Signaling Technology, 3547), Rab7 (Cell Signaling Technology, 9367), Rab9 (Cell Signaling Technology, 5118), Rab11 (Cell Signaling Technology, 5589), pSTAT3 (Y705) (Cell Signaling Technology, 9145), STAT3 (Cell Signaling Technology, 9139), p62 (Cell Signaling Technology, 8025), LC3 (Cell Signaling Technology, 3868), HSP70 (Cell Signaling Technology, 4876), LAMP-1 (BD Biosciences, Franklin Lakes, NJ, USA, 611042), LAMP-2 (Sigma-Aldrich, L0668), and beta-actin (Merck Millipore, MAB1501).

After incubation with the primary antibody, the membranes were probed with the corresponding horseradish peroxidase-conjugated secondary antibody (1:10,000 dilution; BioLegend, San Diego, CA, USA) for one hour at room temperature. Protein bands were visualized using an ECL solution (Thermo Fisher Scientific) and imaged using a ChemiDocTM Imaging System (Bio-Rad, Hercules, CA, USA). Quantification of protein expression levels was performed using Image J software (V1.53c, NIH, Bethesda, MD, USA). For cell and tissue lysates, protein levels were normalized to β-actin or the corresponding total protein, as appropriate. CSF samples were analyzed separately as described in the Human cerebrospinal fluid section above.

For validation of the exogenously expressed 2N4R tau band, recombinant human 2N4R tau (Abcam, ab84700) was used as a positive control, and lysates from empty-vector-transfected HEK293 and SH-SY5Y cells were used as negative controls.

Human phosphorylated tau and amyloid-β42 ELISA

Conditioned media from the experimental samples were analyzed using human phosphorylated tau (T181/S396) and amyloid-β42 ELISA kits (Invitrogen) according to the manufacturer's instructions. Standards for each assay were prepared by diluting the corresponding supplied standard with standard dilution buffer to a concentration of 2,000 pg/ml, followed by serial dilutions to achieve concentrations ranging from 31.25 to 1,000 pg/ml. Duplicate wells received 100 µl of the corresponding standards, whereas sample wells received 50 µl of standard dilution buffer and 50 µl of sample in duplicate. After incubation for 2 h at room temperature on a rotary shaker, the plates were washed four times. Subsequently, 100 µl of the corresponding detection antibody for phosphorylated tau or amyloid-β42 was added to each well and incubated for 1 h, followed by four washes. The corresponding HRP conjugate was then added according to the manufacturer's instructions and incubated for 30 min. Subsequently, 100 µl of stabilized chromogen was added to each well, and the plates were incubated at room temperature in darkness for 20 min on a rotary shaker. The reactions were stopped with 100 µl of the provided stop solution, and absorbance was measured at 450 nm using a SPECTRA MAX 190 plate reader (Molecular Devices, San Jose, CA, USA).

Immunoprecipitation

Cells were lysed in NP-40 lysis buffer (0.5% NP-40, 10 mM Tris–HCl [pH 8.0], 150 mM NaCl, 10 mM sodium pyrophosphate, and 1 mM EDTA) supplemented with 1 mM NaF, 1 mM Na3VO4, and protease inhibitor cocktail. Antibodies were pre-conjugated to magnetic beads (DYNAL, Invitrogen) for 3 h at 4°C. Equal amounts of lysates were then added to the antibody-conjugated beads and incubated overnight at 4°C. After overnight incubation at 4 °C, the beads were washed thrice with NETN wash buffer (0.1% NP-40, 50 mM Tris–HCl [pH 8.0], 150 mM NaCl, 1 mM EDTA). The beads were then boiled in 1× SDS-sample loading buffer and 1× reducing agent at 95 °C for 5 min. Proteins were subsequently separated by SDS-PAGE and immunoblotted under reducing and non-reducing conditions as previously described.

Fluorescent imaging

The HEK293 and SH-SY5Y cells were fixed in 2% paraformaldehyde (Sigma-Aldrich) for 15 min, followed by overnight incubation with primary antibodies, including PHF-1, Tau5, Tau (Dako), and FAM84B in gelatin blocking buffer [0.1% gelatin (Sigma-Aldrich), 0.3% Triton X-100 (Thermo Fisher Scientific), 16 mM sodium phosphate (Sigma-Aldrich), 450 mM NaCl (Sigma-Aldrich), pH 7.4] at 4°C. After three washes with 1× PBS, the cells were incubated with Alexa Fluor 405/488/568-conjugated secondary antibodies (Invitrogen) for 2 h at room temperature. Following additional washes with 1× PBS, the cells were counterstained and mounted using the ProLong Gold Antifade Reagent (Thermo Fisher Scientific).

To detect fluorescently tagged proteins, including GFP-tau and mCherry-FAM84B, cells were fixed in 2% paraformaldehyde for 15 min. After three washes with 1× PBS, the cells were counterstained and mounted using the ProLong Gold Antifade Reagent.

iPSC-derived cortical neurons were fixed in 4% paraformaldehyde (Biosesang, Seongnam, Korea) for 20 min, permeabilized in phosphate-buffered saline (PBS; GeneDEPOT) containing 0.25% Triton X-100 (Sigma-Aldrich) for 10 min, and blocked with 5% bovine serum albumin (BSA; Sigma-Aldrich) for 30 min. Cells were incubated overnight at 4 °C with primary antibodies, including PHF-1 (Peter Davies Lab), Tau (Santa Cruz Biotechnology, Dallas, TX, USA, sc-32274), and FAM84B (OriGene, TA501992; Proteintech, 18421-1-AP). Subsequently, the cells were incubated with Alexa Fluor 488/594-conjugated secondary antibodies (Invitrogen) for one hour at room temperature. Nuclei were counterstained with 4',6-diamidino-2-phenylindole (DAPI; Thermo Fisher Scientific) and mounted using Faramount Aqueous Mounting Medium (Dako).

Brain organoids were fixed in 4% paraformaldehyde (Biosesang) for one hour, washed with PBS, embedded in O.C.T. (Tissue-Tek, Sakura Finetek USA, Inc., Torrance, CA, USA), and cryosectioned into 10-µm-thick slices. Immunocytochemistry was performed on the slices using the method described for cortical neurons.

Fluorescent images were captured using an EVOS M5000 Imaging System (Invitrogen), FV3000 microscope (Olympus, Tokyo, Japan), and LSM880 microscope (Carl Zeiss AG, Oberkochen, Germany). Colocalization was quantified using Pearson's correlation coefficient calculated with the Coloc2 plugin in ImageJ (V1.53c, NIH).

Statistical analyses

Data are presented as mean ± standard error of the mean unless specified otherwise. For applicable cell-based experiments, samples were randomly assigned to control or experimental groups, and the investigators were blinded to the experimental conditions. None of the samples were excluded from the analyses. For human tissue and CSF analyses, n denotes individual donors or participants, respectively. For biochemical cell-culture experiments, n denotes independent cultures, transfections, or differentiations, as specified in the figure legends. For imaging analyses, fields of view obtained from the same independent culture were treated as subsamples and averaged before inferential statistical analysis. Normal distribution and homogeneity of variance within each comparison group were assessed prior to statistical analysis. Statistical comparisons between two groups were performed using an unpaired two-tailed *t*-test with Welch's correction for unequal variances. For experiments involving simultaneous comparisons among three or more groups, ordinary one-way ANOVA followed by Tukey's or Dunnett's multiple-comparisons test was used, as appropriate. Statistical significance was set at $p < 0.05$.

Results

FAM84B levels show a context-dependent association with tau

HEK293 cell lines stably expressing wild-type 2N4R tau were generated as an initial tau-overexpression model under G418 selection. Among the isolated clones, one clone with relatively high intracellular tau levels and one with relatively low tau levels were selected for an initial gene-expression comparison. Microarray analysis identified several differentially expressed genes (DEGs) between the two clones (Supplementary Fig. 1). Notably, FAM84B transcript levels were approximately 18-fold lower in the selected high-tau clone than in the low-tau clone.

To extend this initial observation to human disease contexts, we next examined FAM84B levels in postmortem cortical tissues from healthy control (HC) donors and donors with VD, CBD, PSP, PART, or AD, as well as in cerebrospinal fluid (CSF) samples from HC participants and participants with MCI or AD. Clinical and neuropathological characteristics of the postmortem donors are summarized in Supplementary Table 1A, and demographic characteristics of the CSF participants are provided in Supplementary Table 1B. In postmortem cortex, FAM84B levels were numerically higher in CBD ($p = 0.0545$) and significantly higher in PSP, PART, and AD than in HC, whereas no significant difference was observed in VD (Fig. 1A and Supplementary Fig. 2A, B). Mean relative FAM84B immunoreactivity in CSF was also numerically higher in MCI and AD than in HC, although these differences did not reach statistical significance (Fig. 1B). Thus, FAM84B showed divergent patterns across experimental and human contexts: FAM84B transcript levels were lower in the selected high-tau clone, whereas FAM84B protein levels were higher in postmortem cortical tissues from several tauopathy groups. This apparent divergence prompted us to examine whether FAM84B influences the cellular distribution of tau.

FAM84B promotes extracellular tau release

To investigate the effect of FAM84B overexpression on intracellular tau levels, HEK293 and SH-SY5Y cells were co-transfected with constructs encoding human 2N4R tau and FAM84B. FAM84B overexpression significantly reduced intracellular phosphorylated tau (PHF-1, S396/S404) and total tau in both cell lines (Fig. 1C), irrespective of the quantity of tau introduced (Supplementary Fig. 3A). Because exogenously expressed 2N4R tau appeared predominantly as a single immunoreactive band, its identity was verified using recombinant human 2N4R tau, empty-vector-transfected cells, and independent tau antibodies. Recombinant and cell-expressed 2N4R tau showed a predominant band at a similar apparent molecular weight, whereas this signal was scarcely seen in vector-transfected controls (Supplementary Fig. 3B). Additional experiments using mouse neuroblastoma cells (Neuro-2A) and human neuroblastoma cells (SH-SY5Y), as well as their differentiated forms, also showed that FAM84B overexpression led to a significant decrease in intracellular phosphorylated tau and total tau protein levels in all tested cell models (Fig. 1C and Supplementary Fig. 3C).

We next examined whether this relationship was also present in human induced pluripotent stem cell (iPSC)-derived cortical neurons. In AD iPSC-derived cortical neurons, FAM84B levels were increased, whereas intracellular phosphorylated tau and total tau levels were reduced, compared with control iPSC-derived cortical neurons (Fig. 1D). These findings showed an association between increased FAM84B and reduced intracellular tau.

We then examined whether the FAM84B-associated reduction in intracellular tau was accompanied by changes in MAPT mRNA or in the abundance of the autophagy- and lysosome-associated proteins. FAM84B overexpression did not affect MAPT mRNA levels in tau-expressing cells (Supplementary Fig. 4A) and reduced total tau protein levels in a doxycycline-inducible tau (DIT) overexpression system in mouse cortical neurons (Supplementary Fig. 4B). Additionally, increased levels of FAM84B did not affect the levels of proteins associated with autophagy and lysosomal degradation (p62, LC3, HSP70, LAMP-1, and LAMP-2) in tau-expressing cells (Supplementary Fig. 4C, D). These observations prompted us to test whether increased extracellular release contributed to the reduction in intracellular tau.

Notably, FAM84B overexpression increased the extracellular release of phosphorylated (T181, S396) and total tau from tau-expressing cells (Fig. 1E), and both tau and FAM84B were detected in conditioned medium from tau-expressing SH-SY5Y cells (Supplementary Fig. 5A). Conditioned medium from AD iPSC-derived cortical neurons contained higher phosphorylated tau (T181, S396) levels than that from control iPSC-derived cortical neurons (Fig. 1F).

We next examined whether the FAM84B-associated changes observed with wild-type 2N4R tau were also reproduced with P301L mutant tau. FAM84B similarly reduced intracellular phosphorylated and total P301L tau while increasing extracellular phosphorylated and total P301L tau (Supplementary Fig. 5B–D). We then compared wild-type and P301L tau to determine whether the intracellular tau-lowering effect of FAM84B showed variant specificity. FAM84B reduced intracellular phosphorylated and total tau across both wild-type and P301L constructs, with no apparent variant-specific pattern (Supplementary Fig. 5E). We further examined whether this effect was restricted to particular tau phosphorylation sites. FAM84B reduced intracellular monomeric and oligomeric tau phosphorylated at T181, T231, S262, and S396/S404, while increasing tau phosphorylated at T181, T231, and S262 in EV-enriched fractions (Supplementary Fig. 5F, G). Together, these findings indicate that the FAM84B-associated redistribution of tau was not restricted to a particular tau variant or phosphorylation site among those examined.

To investigate the effects of FAM84B deletion on extracellular tau release, FAM84B-knockout HEK293 cells were generated (Supplementary Fig. 6A). In FAM84B-knockout HEK293 cells, extracellular phosphorylated and total tau levels were reduced for both wild-type and P301L mutant 2N4R tau, whereas intracellular levels of the tested tau constructs were increased (Supplementary Fig. 6B–D). Together, the gain- and loss-of-function results support a role for FAM84B in redistributing tau from the intracellular compartment toward extracellular release rather than simply reducing intracellular tau abundance.

FAM84B associates with EV-enriched fractions and promotes tau transfer

To examine the spatial association between FAM84B and 2N4R tau, we used fluorescently tagged constructs and immunocytochemistry in multiple tau-expressing cellular models. In cells expressing GFP-tau and mCherry-FAM84B, we observed their colocalization as intracellular and extracellular granules (Fig. 1G and Supplementary Fig. 7A, B, G). Immunocytochemistry further showed colocalization between FAM84B and phosphorylated and total tau across multiple cell models, including AD iPSC-derived cortical neurons (Fig. 1H and Supplementary Fig. 7C–G). This colocalization prompted us to examine whether FAM84B and tau associate through a stable protein–protein interaction or within vesicle- or lipid-associated extracellular complexes.

Immunoprecipitation assays were performed using lysates and culture media from cells overexpressing 2N4R tau and FAM84B, to explore the presence of interactions. No FAM84B-tau coprecipitation was detected in cell lysates prepared in the presence of the detergent NP-40 (Supplementary Fig. 8A). However, a high-molecular-weight tau-immunoreactive species coprecipitated with FAM84B in culture media under detergent-free conditions (Supplementary Fig. 8B). Following boiling in the presence of a reducing agent, this high-molecular-weight signal resolved to a band at the apparent molecular weight of monomeric tau (Supplementary Fig. 8C). Together with the loss of FAM84B–tau coprecipitation following NP-40 treatment (Supplementary Fig. 8D), these findings are consistent with the presence of tau and FAM84B in a detergent-sensitive extracellular complex rather than a stable protein–protein interaction.

To determine whether extracellular FAM84B and 2N4R tau were associated with EV-enriched material, we examined membrane-affinity-isolated fractions from conditioned medium using multiple EV-associated and non-EV markers. Alix, TSG101, CD9, CD63, and CD81 were detected in the isolated fractions, whereas calnexin showed minimal immunoreactivity in the isolated fractions (Fig. 2A). These findings support enrichment of EV-associated material in the isolated fractions. Consistent with these biochemical findings, fluorescence imaging showed colocalization of FAM84B with the EV-associated protein Alix in tau- and FAM84B-expressing SH-SY5Y cells (Fig. 2B). FAM84B, phosphorylated tau, and total tau co-fractionated with these EV-enriched

preparations. Membrane protein isolation further revealed that FAM84B was associated with the membrane fraction together with caveolin-1 (Fig. 2C). Collectively, these findings support an association of FAM84B and tau with EV-enriched extracellular fractions.

To further elucidate the role of FAM84B in tau transfer, we employed two complementary cell-based tau-transfer assays and an organoid-based spatial colocalization analysis (Fig. 2D–F). First, we exposed naïve recipient cells to conditioned medium collected from donor cells expressing 2N4R tau alone or co-expressing tau and FAM84B to determine whether tau uptake occured (Fig. 2D). Our findings showed significantly greater uptake of phosphorylated and total tau in HEK293 and SH-SY5Y recipient cells exposed to conditioned medium from cells co-expressing FAM84B and tau than in cells exposed to conditioned medium from cells expressing tau alone (Fig. 2G, H, and Supplementary Fig. 9A–C). Recipient cells exposed to conditioned medium from tau- and FAM84B-coexpressing donor cells showed greater colocalization of FAM84B with phosphorylated and total tau than cells exposed to tau-only conditioned medium.

Next, we investigated cell-to-cell tau transfer when FAM84B was overexpressed in cells transfected with a tau transfer reporter construct (Tau-p2a-eGFP) (Fig. 2E). FAM84B overexpression significantly increased the number of GFP-negative/PHF-1-positive recipient cells without significantly altering the number of GFP-positive donor cells (Fig. 2I, J).

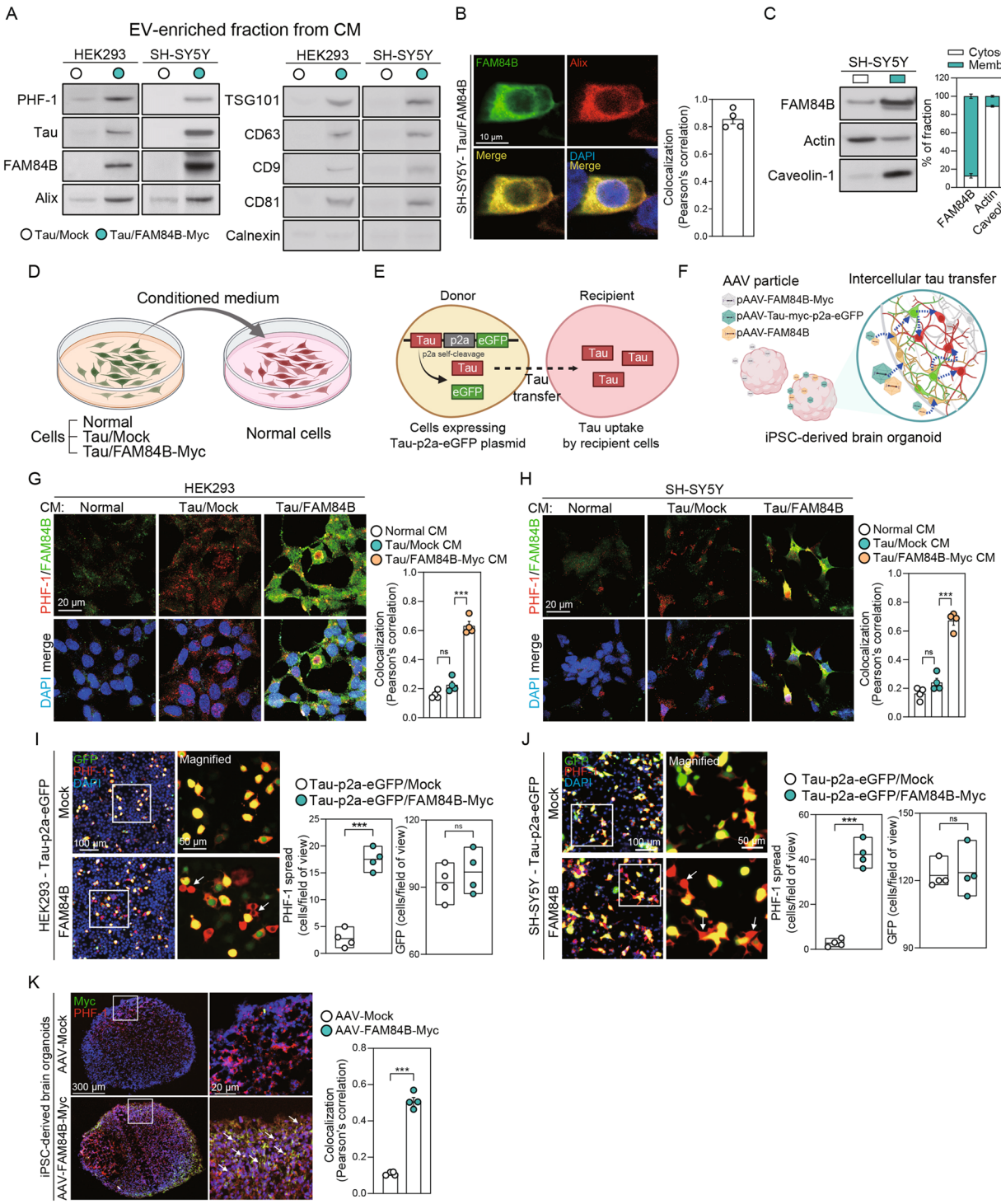
Finally, we examined the spatial association between FAM84B and phosphorylated tau in brain organoids transduced with AAV-FAM84B (Fig. 2F). The outer region of AAV-FAM84B-transduced organoids showed prominent colocalization between FAM84B and phosphorylated tau compared with control organoids (Fig. 2K). Collectively, these results support an association of FAM84B and tau with EV-enriched fractions and show that FAM84B promotes tau transfer in cell-based assays, while the organoid model demonstrates their spatial colocalization.

FAM84B-associated tau transfer involves ryanodine receptor 3-linked calcium signaling and a clathrin-associated endocytic component

To investigate the mechanism underlying FAM84B-associated extracellular secretion, we performed mRNA-seq analysis using RNA extracted from cells with FAM84B deletion, FAM84B overexpression, or simultaneous overexpression of FAM84B and tau (Fig. 3A–C). Comparison of the three datasets identified shared differentially expressed genes that mapped to membrane-related Gene Ontology cellular component categories (Fig. 3D, E). These findings were consistent with a potential role for FAM84B in membrane-associated trafficking.

Among the genes with altered expression patterns, ryanodine receptor 3 (RYR3) consistently appeared in all three mRNA-seq datasets. The direction of RYR3 expression changes across these comparisons was consistent with FAM84B perturbation, prompting us to further examine RYR3 as a candidate downstream component of FAM84B-associated signaling. In pooled analyses of the two AD iPSC-derived cortical neuron lines, RYR3 levels were increased compared with pooled control lines (Fig. 3F). In a similar manner, there was a notable increase in RYR3 levels among SH-SY5Y cells overexpressing tau and FAM84B relative to that in cells expressing tau alone (Fig. 3G).

RYR3 functions as an endoplasmic reticulum calcium-release channel, while elevations in cytosolic calcium are known to regulate exocytosis [26, 27]. Fluo-4 AM imaging revealed greater spatial overlap between mCherry-FAM84B and calcium-sensitive Fluo-4 fluorescence in 2N4R tau- and FAM84B-coexpressing cells than in control cells (Fig. 3H and Supplementary Fig. 10A). This overlap was markedly reduced by dantrolene, indicating that the FAM84B-associated calcium signal was sensitive to ryanodine receptor inhibition. To further define the contribution of RYR3, we complemented this pharmacological approach with RYR3-targeting siRNA. RYR3 siRNA reduced RYR3 protein levels to approximately 20% of control levels in tau- and FAM84B-expressing SH-SY5Y cells (Supplementary Fig. 11A). RYR3 knockdown significantly reduced the spatial overlap between FAM84B and Fluo-4 fluorescence compared with control siRNA, although the effect was smaller than that observed with dantrolene (Supplementary Fig. 11B).



To examine the contribution of ryanodine receptor signaling to FAM84B-associated 2N4R tau transfer, we treated cells co-expressing Tau-p2a-eGFP and FAM84B with dantrolene. Dantrolene treatment markedly reduced the FAM84B-associated tau transfer (Fig. 3I and Supplementary Fig. 10B), supporting a contribution of ryanodine receptor signaling to this process. We next examined whether RYR3 knockdown also affected tau transfer. RYR3 knockdown significantly reduced FAM84B-associated tau transfer compared with control siRNA, although the effect was smaller than that observed with dantrolene (Supplementary Fig. 11C). These findings

Fig. 2 FAM84B promotes extracellular tau release and intercellular transfer with an EV-associated component. **A** Immunoblots showing levels of PHF-1, total tau, FAM84B, Alix, TSG101, CD9, CD63, CD81, and calnexin in EV-enriched fractions isolated from the CM of HEK293 and SH-SY5Y cells expressing tau alone or tau with FAM84B-Myc (n=3 each). **B** Colocalization of FAM84B and Alix in SH-SY5Y cells expressing tau with FAM84B (n=4). **C** Relative levels of FAM84B, actin, and caveolin-1 in cytosolic and membrane fractions of SH-SY5Y cells expressing tau with FAM84B (n=3). **D** Illustration describing the administration of CM from normal cells, cells expressing tau alone, and cells expressing tau with FAM84B-Myc into normal cells, supporting the results shown in (**G**) and (**H**). **E** Illustration depicting tau transmission from Tau-p2a-eGFP expressing cells (donor) to neighboring cells (recipient), supporting the results shown in (**I**) and (**J**). **F** Illustration of the AAV-based brain-organoid experiment used to examine the spatial association between FAM84B and phosphorylated tau, supporting the results shown in (**K**). **G** Uptake and colocalization of PHF-1 and FAM84B in HEK293 cells exposed to CM from normal cells, cells expressing tau alone, and cells expressing tau with FAM84B-Myc (n=4 each). **H** Uptake and colocalization of PHF-1 and FAM84B in SH-SY5Y cells exposed to CM from normal cells, cells expressing tau alone, and cells expressing tau with FAM84B-Myc (n=4 each). **I** PHF-1 transfer from Tau-p2a-eGFP expressing HEK293 cells to neighboring cells in response to FAM84B expression (n=4 each). Arrows indicate recipient cells (red) to which tau has been transmitted. Solid boxes in the images indicate magnified areas. **J** PHF-1 transfer from Tau-p2a-eGFP expressing SH-SY5Y cells to neighboring cells in response to FAM84B expression (n=4 each). Arrows indicate recipient cells (red) to which tau has been transmitted. Solid boxes in the images indicate magnified areas. **K** Colocalization (arrow) of PHF-1 and FAM84B (Myc) in iPSC-derived brain organoids from HC infected with AAV containing control vector or FAM84B-Myc (n=4 each). Solid boxes in the images indicate magnified areas. Results are presented as mean ± SEM. Colocalization analysis: (**B**, **G**, **H**, **K**) Pearson's correlation coefficient. Statistical analyses: (**G**, **H**) ordinary one-way ANOVA followed by Tukey's multiple-comparisons test; (**I**–**K**) unpaired two-tailed t-test with Welch's correction; ns: not significant; ***$p < 0.001$. Illustration (**D**-**F**) was created with BioRender.com (Agreement number: XO2789HRIK, RF2789HV9J, VS2789HBYY). Abbreviations: PHF-1, phosphorylated tau at residues S396/S404; EV, extracellular vesicle; CM, conditioned medium; HC, healthy control; AAV, adeno-associated virus

support a contributory role for RYR3 in FAM84B-associated calcium signaling and tau transfer, but do not establish RYR3 as the sole mediator of this process.

To explore the mechanism underlying the uptake of extracellular FAM84B- and 2N4R tau-associated material by neighboring cells, the levels of endocytosis-associated proteins such as clathrin and caveolin and endosomal markers in cells co-expressing FAM84B and tau were compared to the levels in cells expressing tau alone. Elevated FAM84B expression significantly upregulated clathrin heavy chain (CHC) levels and downregulated caveolin-1 levels in tau-expressing cells compared to cells expressing tau alone (Fig. 4A). However, there were no discernible changes observed in early or late endosomal marker proteins (EEA1, RAB5, RAB7, RAB9, and RAB11) compared to controls. Increased CHC levels were also observed in the postmortem cerebral cortex of donors with PSP and AD and in AD iPSC-derived cortical neurons compared with their respective controls (Fig. 4B, C).

To pharmacologically examine the contribution of endocytic uptake to FAM84B-associated 2N4R tau transfer, we treated cells with Pitstop2, an inhibitor of clathrin-associated endocytosis. Compared to DMSO-treated controls, Pitstop2 increased extracellular tau and FAM84B levels, reduced their intracellular levels, and substantially attenuated tau transfer (Fig. 4D–G). These pharmacological findings supported the involvement of endocytic uptake but, because Pitstop2 is not specific for clathrin-mediated endocytosis and can affect additional endocytic pathways, did not establish pathway specificity.

We therefore directly examined the contribution of CHC using siRNA-mediated knockdown. CHC siRNA reduced CHC protein levels to approximately 10% of control levels in 2N4R tau- and FAM84B-expressing SH-SY5Y cells (Supplementary Fig. 11D). CHC knockdown altered extracellular tau/FAM84B levels and attenuated FAM84B-associated tau transfer, although the effects were smaller than those observed with Pitstop2 (Supplementary Fig. 11E, F). These results support a contribution of CHC-associated uptake to FAM84B-associated tau transfer but do not indicate that clathrin represents the exclusive route of tau internalization.

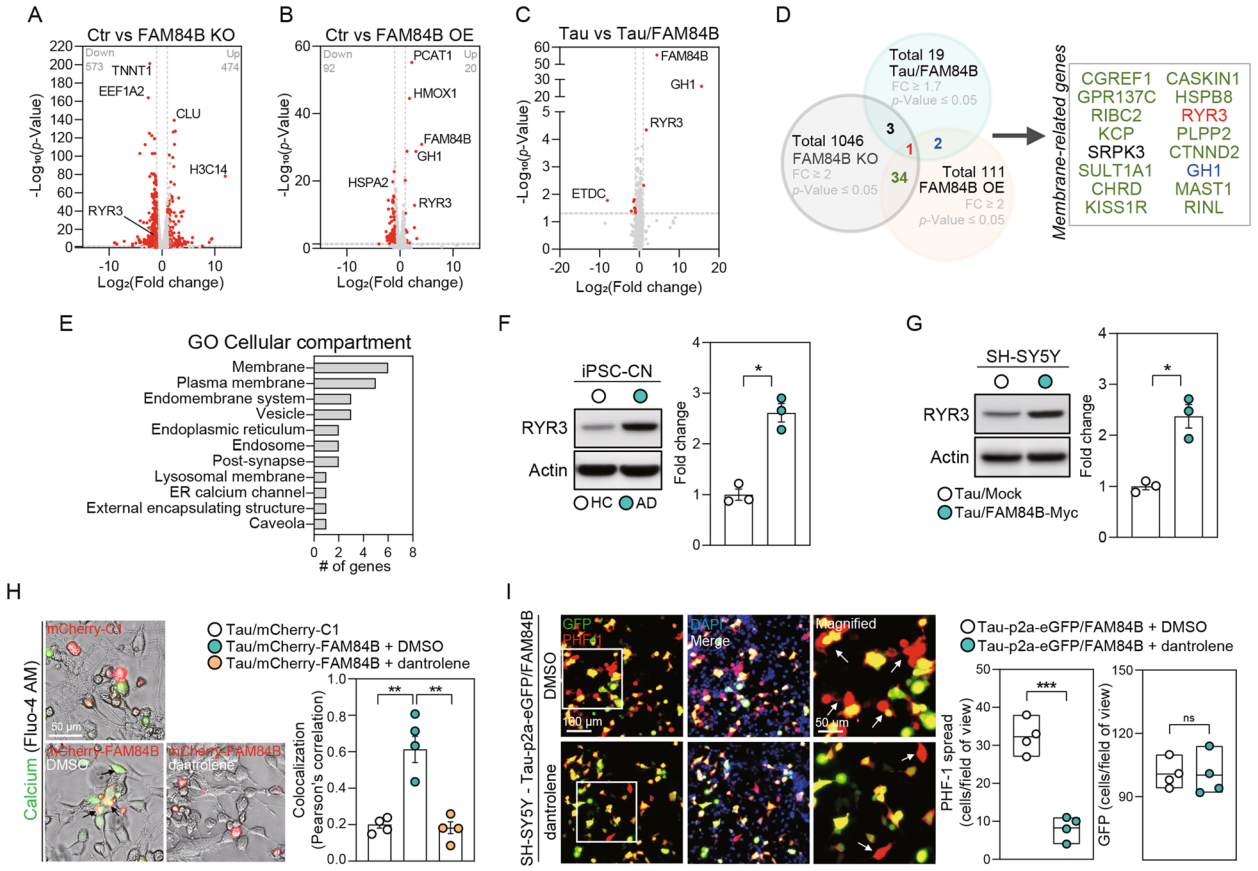


Fig. 3 FAM84B-associated tau transfer involves RYR3-linked calcium signaling. **A** Differentially expressed genes in HEK293 cells in response to FAM84B KO (n=3 each). Genes with $p < 0.05$ and >2-fold expression change compared to control are marked with red dots. **B** Differentially expressed genes in HEK293 cells in response to FAM84B OE (n=3 each). Genes with $p < 0.05$ and >2-fold expression change compared to control are marked with red dots. **C** Differentially expressed genes in tau-expressing SH-SY5Y cells in response to FAM84B OE (n=3 each). Genes with $p < 0.05$ and >1.7-fold expression change compared to cells expressing tau alone are marked with red dots. **D** Venn diagram showing the number of shared genes between RNA-seq datasets in (**A**–**C**), with overlapping genes represented in distinct colors (red, green, black, blue). Only the names of membrane-related genes among the shared genes are noted. **E** GO analysis showing cellular compartments of genes identified in (**D**). The GO terms based on the number of genes are shown. **F** Levels of RYR3 and actin in iPSC-derived CN from HC and patients with AD (n=3 each). HC and AD data represent physically pooled samples of the two respective iPSC lines. **G** Levels of RYR3 and actin in SH-SY5Y cells expressing tau alone or tau with FAM84B-Myc (n=3 each). **H** Colocalization (arrow) of FAM84B and calcium in SH-SY5Y cells expressing tau with mCherry control (C1), and in cells expressing tau with mCherry-FAM84B treated with either DMSO or dantrolene (n=4 each). **I** PHF-1 transfer from SH-SY5Y cells expressing Tau-p2a-eGFP with FAM84B to neighboring cells in response to treatment with either DMSO or dantrolene (n=4 each). Arrows indicate recipient cells (red) to which tau has been transmitted. Solid boxes in the images indicate magnified areas. Results are presented as mean ± SEM. Colocalization analysis: (**H**) Pearson's correlation coefficient. Statistical analyses: Differential expression analyses in (**A**-**C**) were performed using Cuffdiff as described in the Methods; (**H**) ordinary one-way ANOVA followed by Tukey's multiple-comparisons test; (**F**, **G**, **I**) unpaired two-tailed t-test with Welch's correction; ns: not significant, *$p < 0.05$, **$p < 0.01$, ***$p < 0.001$. Abbreviations: KO, knockout; OE, overexpression; GO, gene ontology; CN, cortical neuron; HC, healthy control; AD, Alzheimer's disease; PHF-1, phosphorylated tau at residues S396/S404

Inflammatory cytokine signaling promotes FAM84B expression and tau transfer

Intrigued by the observed upregulation of FAM84B in the postmortem cerebral cortex of tauopathy patients (Fig. 1A), we analyzed ChIP-seq data (ENCODE, ChEA) for transcription factors binding to the FAM84B promoter in order to identify the regulators of FAM84B expression. We identified several transcription regulators

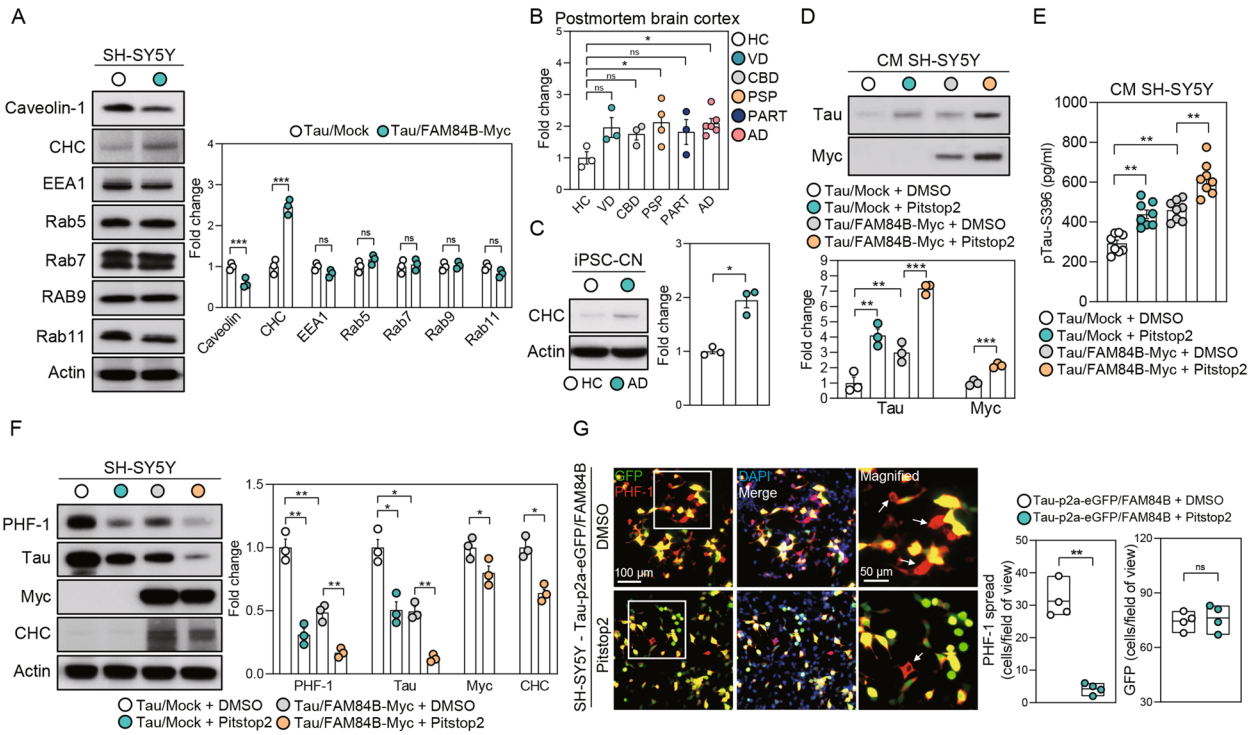


Fig. 4 FAM84B-associated tau transfer involves a clathrin-associated endocytic component. **A** Levels of caveolin-1, CHC, EEA1, RAB5, RAB7, RAB9, RAB11, and actin in SH-SY5Y cells expressing tau alone or tau with FAM84B-Myc (n=3 each). **B** CHC levels in the cerebral cortex of HC (n=3) and patients with VD (n=3), CBD (n=3), PSP (n=4), PART (n=3), and AD (n=6). **C** Levels of CHC and actin in iPSC-derived CN from HC and patients with AD (n=3 each). HC and AD data represent physically pooled samples of the two respective iPSC lines. **D** Changes in the levels of tau and FAM84B (Myc) in the CM from SH-SY5Y cells expressing tau alone or tau with FAM84B-Myc after treatment with either DMSO or Pitstop2 (n=3 each). **E** Changes in the levels of phosphorylated tau (S396) in the CM from SH-SY5Y cells expressing tau alone or tau with FAM84B-Myc after treatment with either DMSO or Pitstop2 (n=8 each). **F** Changes in the levels of PHF-1, total tau, FAM84B (Myc), CHC, and actin in SH-SY5Y cells expressing tau alone or tau with FAM84B-Myc after treatment with either DMSO or Pitstop2 (n=3 each). **G** PHF-1 transfer from SH-SY5Y cells expressing Tau-p2a-eGFP with FAM84B to neighboring cells in response to treatment with either DMSO or Pitstop2 (n=4 each). Arrows indicate recipient cells (red) to which tau has been transmitted. Solid boxes in the images indicate magnified areas. Results are presented as mean ± SEM. Statistical analyses: (**B**, **D**-**F**) ordinary one-way ANOVA followed by Tukey's multiple-comparisons test; (**A**, **C**, **G**) unpaired two-tailed t-test with Welch's correction; ns: not significant, *$p < 0.05$, **$p < 0.01$, ***$p < 0.001$. Abbreviations: CHC, clathrin heavy chain; HC, healthy control; VD, vascular dementia; CBD, corticobasal degeneration; PSP, progressive supranuclear palsy; PART, primary age-related tauopathy; AD, Alzheimer's disease; CN, cortical neuron; CM, conditioned medium; PHF-1, phosphorylated tau at residues S396/S404

involved in inflammation (STAT3 and JUN), hormone signaling (ESR1), and chromatin remodeling (SUZ12, RNF2, ZNF217, and PHF8) (Fig. 5A). STAT3 binding was observed in association with the FAM84B enhancer, whereas ESR1 and JUN were associated with nearby regulatory elements (Fig. 5B). Increased STAT3 activity via Y705 phosphorylation was observed in several tauopathy groups in postmortem cerebral cortex and in AD iPSC-derived cortical neurons compared with controls (Fig. 5C, D and Supplementary Fig. 12A, B).

Proinflammatory cytokines, and notably interleukin (IL)−6, reliably phosphorylate STAT3 at Y705 [28]. Treatment of SH-SY5Y cells with IL-6 increased levels of STAT3 phosphorylation at Y705 and FAM84B compared to those in untreated controls (Fig. 5E). This effect was consistent in IL-6-treated cells expressing wild-type STAT3 but absent in cells with a dominant-negative STAT3 mutation, indicating that FAM84B expression is regulated by IL-6-mediated STAT3 activation (Fig. 5F). Tumor necrosis factor (TNF)-α treatment was also associated with increased FAM84B levels in SH-SY5Y cells (Supplementary Fig. 12C). Intercellular tau transfer was elevated in cells expressing Tau-p2a-eGFP and treated with IL-6 or TNF-α compared to controls (Fig. 5G and Supplementary

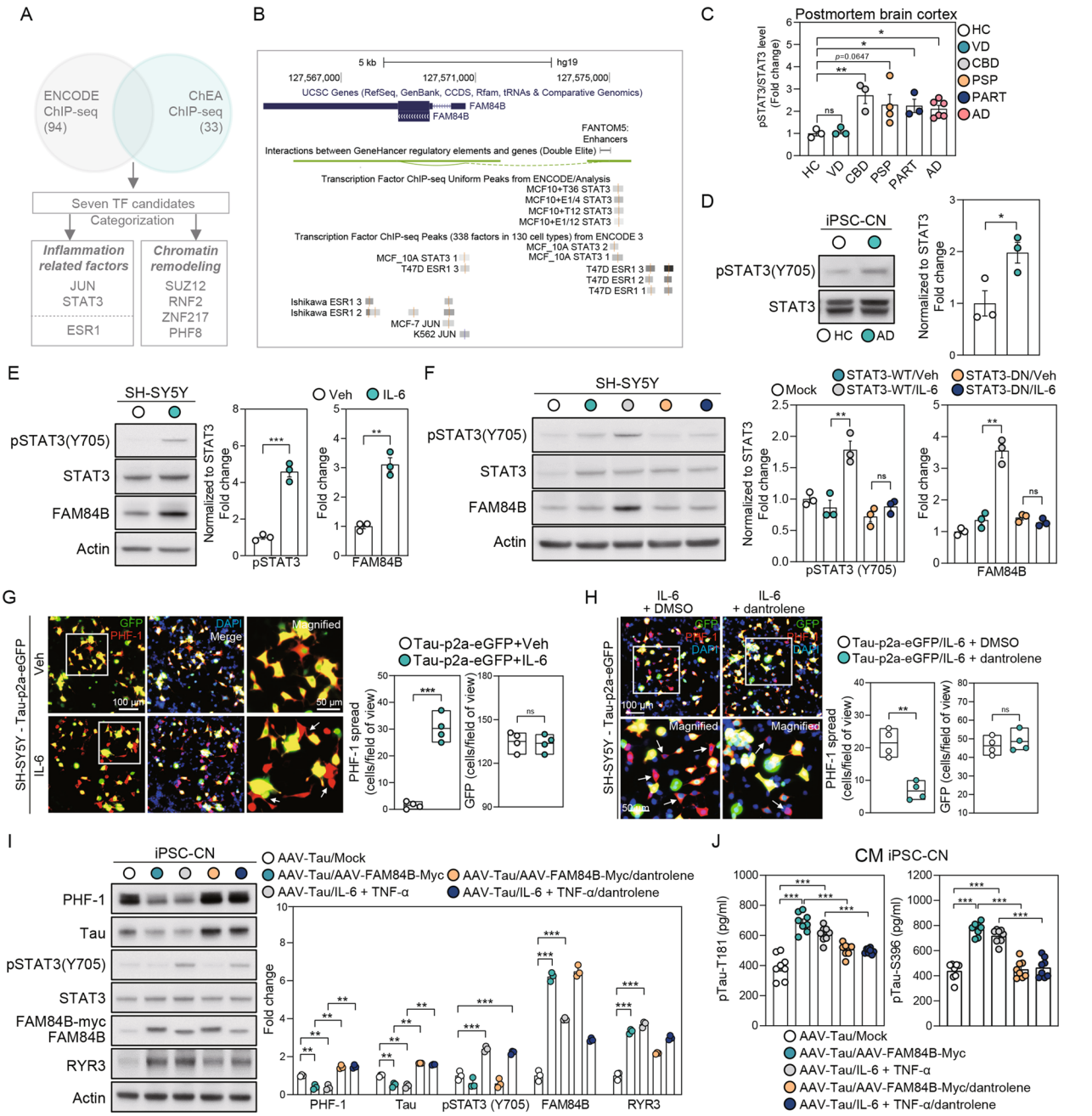


Fig. 12D). These findings suggest that neuroinflammatory cytokine signaling can increase FAM84B expression and promote tau transfer.

We next examined the relationship among neuroinflammatory signaling, FAM84B, ryanodine receptor-linked calcium signaling, and 2N4R tau transfer in SH-SY5Y cells and iPSC-derived cortical neurons. In SH-SY5Y cells expressing Tau-p2a-eGFP, dantrolene significantly suppressed the IL-6-induced increase in tau transfer compared with DMSO-treated cells (Fig. 5H). These results support a contribution of ryanodine receptor-linked calcium signaling to IL-6-associated tau transfer.

We extended these observations to iPSC-derived cortical neurons expressing AAV-Tau together with either control AAV or AAV-FAM84B-Myc, as well as to AAV-Tau-expressing neurons treated with IL-6 and TNF-α. Corresponding FAM84B- and cytokine-treated groups were additionally treated with dantrolene. RYR3 levels increased significantly in iPSC-derived cortical neurons expressing FAM84B via AAV infection and in those

Fig. 5 Inflammatory cytokine signaling promotes FAM84B expression and tau transfer. **A** Venn diagram showing the seven shared transcriptional regulators between the ENCODE ChIP-seq and ChEA ChIP-seq datasets. The genes are categorized into functional terms and noted. **B** Genomic information of the FAM84B gene obtained from the UCSC Genome Browser. Transcription cofactor clusters identified from the ENCODE ChIP-seq data, with those likely to bind to the regulatory elements of FAM84B, as identified by FANTOM5, highlighted. **C** Levels of phosphorylated STAT3 (Y705) in the cerebral cortex of HC (n=3) and patients with VD (n=3), CBD (n=3), PSP (n=4), PART (n=3), and AD (n=6). **D** Levels of phosphorylated STAT3 (Y705) and total STAT3 in iPSC-derived CN from HC and patients with AD (n=3 each). HC and AD data represent physically pooled samples of the two respective iPSC lines. **E** Levels of phosphorylated STAT3 (Y705), total STAT3, FAM84B, and actin in SH-SY5Y cells treated with either control vehicle or IL-6 (n=3 each). **F** Changes in the levels of phosphorylated STAT3 (Y705), total STAT3, FAM84B, and actin in SH-SY5Y cells expressing STAT3-WT or STAT3-DN in response to treatment with either control vehicle or IL-6 (n=3 each). **G** PHF-1 transfer from Tau-p2a-eGFP expressing SH-SY5Y cells to neighboring cells in response to treatment with either control vehicle or IL-6 (n=4 each). Arrows indicate recipient cells (red) to which tau has been transmitted. Solid boxes in the images indicate magnified areas. **H** PHF-1 transfer from IL-6 treated SH-SY5Y cells expressing Tau-p2a-eGFP to neighboring cells in response to treatment with either DMSO or dantrolene (n=4 each). Arrows indicate recipient cells (red) to which tau has been transmitted. Solid boxes in the images indicate magnified areas. **I** Changes in the levels of PHF-1, total tau, phosphorylated STAT3 (Y705), total STAT3, FAM84B (FAM84B-Myc), RYR3, and actin in iPSC-derived CN from HC after infection with AAV and subsequent treatments (n=3 each). **J** Changes in the levels of phosphorylated tau (T181 and S396) in the CM of iPSC-derived CN from HC after infection with AAV and subsequent treatments (n=8 each). In (I-J), each independent sample was generated by physically pooling equal amounts of material from the two control iPSC lines. In (**I**–**J**), the experimental groups are: (1) CN infected with AAV containing tau, (2) CN infected with AAV containing tau and FAM84B-Myc, (3) CN infected with AAV containing tau and treated with IL-6 and TNF-α, (4) CN infected with AAV containing tau and FAM84B-Myc and treated with dantrolene, and (5) CN infected with AAV containing tau, treated with IL-6 and TNF-α, followed by treatment with dantrolene. Results are presented as mean ± SEM. Statistical analyses: (**C**, **F**, **I**, **J**) ordinary one-way ANOVA followed by Tukey's multiple-comparisons test; (**D**, **E**, **G**, **H**) unpaired two-tailed t-test with Welch's correction; ns: not significant, $*p < 0.05$, $**p < 0.01$, and $***p < 0.001$. Abbreviations: HC, healthy control; VD, vascular dementia; CBD, corticobasal degeneration; PSP, progressive supranuclear palsy; PART, primary age-related tauopathy; AD, Alzheimer's disease; CN, cortical neuron; WT, wild type; DN, dominant negative; PHF-1, phosphorylated tau at residues S396/S404; AAV, adeno-associated virus; CM, conditioned medium

co-treated with IL-6 and TNF-α (Fig. 5I). A reduction in intracellular phosphorylated and total tau levels was consistently observed in iPSC-derived cortical neurons co-expressing tau and FAM84B and in neurons treated with IL-6 and TNF-α (Fig. 5I). These changes were accompanied by increased extracellular phosphorylated tau levels relative to the respective controls (Fig. 5J). Dantrolene treatment attenuated the FAM84B- and cytokine-associated reduction in intracellular phosphorylated and total tau and reduced the corresponding increases in extracellular phosphorylated tau (Fig. 5I, J).

Collectively, these findings indicate that neuroinflammatory signaling is associated with increased FAM84B expression and engagement of an RYR3-linked calcium signaling component that contributes to cell-to-cell tau transfer (Supplementary Fig. 13).

Discussion

In AD, cognitive decline correlates more directly with the accumulation of tau than with amyloid plaque burden [29, 30]. Braak and Braak described a stereotyped spatiotemporal distribution of tau pathology across brain regions, a pattern that has contributed to the concept that pathological tau may spread through interconnected neural systems [31]. Accumulating evidence indicates that neuroinflammation contributes to neurodegeneration [20] and significantly accelerates the aggregation and phosphorylation of tau [32, 33]. Furthermore, reactive microglia are sufficient to drive tau pathology and their presence is correlated with the spread of tau pathology throughout the brain [34]. However, how neuroinflammatory signaling modulates intercellular tau transfer remains incompletely understood.

In the present study, we identified FAM84B as a neuroinflammation-associated regulator of tau redistribution and intercellular transfer. Rather than interpreting intercellular tau transfer as equivalent to seeded pathological

propagation, our findings support a distinction between FAM84B-associated tau export and transfer and subsequent pathological consequences of transferred tau. In this framework, neuroinflammatory stress may engage a FAM84B-associated protein export-and-transfer program that facilitates extracellular release and redistribution of tau to neighboring cells. However, the present data do not establish when this process occurs during the course of human tauopathy or whether it precedes established pathological propagation.

An apparent discrepancy in our findings is that FAM84B expression was markedly reduced in the high-intracellular-tau discovery cell model, whereas FAM84B levels were elevated in postmortem brain tissues from several tauopathies. FAM84B levels were significantly elevated in PSP, PART, and AD and numerically higher in CBD, but were not significantly altered in VD (Fig. 1A), suggesting that FAM84B may play a common role in tauopathy-related pathological backgrounds. We interpret these findings as reflecting distinct temporal and compartmental contexts rather than opposing effects of FAM84B. One possible interpretation is that reduced FAM84B expression in the high-intracellular-tau discovery clone reflected impaired tau export or clone-specific adaptation, thereby favoring intracellular tau retention. In contrast, chronic tauopathy tissues are characterized by sustained disease-associated and neuroinflammatory conditions, which may induce FAM84B expression through STAT3-associated signaling. Under this disease-associated context, increased FAM84B may promote the redistribution of tau from donor cells toward extracellular and recipient-cell compartments. Thus, FAM84B-mediated tau export may reduce intracellular tau burden at the donor-cell level, while potentially increasing extracellular tau availability and intercellular tau exposure at the tissue level. As shown in Figs. 1 and 2, increased FAM84B promotes the redistribution of intracellular tau toward extracellular release and transfer to adjacent cells, which may contribute to tauopathy-associated intercellular tau spread under disease-related inflammatory conditions. Intriguingly, tau overexpression in cells neither induced nor reduced the expression of FAM84B (Supplementary Fig. 3B), and FAM84B itself did not affect the transcription of tau (Supplementary Fig. 4A). Thus, it is speculated that ectopic accumulation of tau in the high-tau discovery clone may have resulted from abnormally low FAM84B expression in the stable cell line, potentially caused by unintended genetic alterations, such as insertional mutations arising during G418 selection. Accordingly, we regard the approximately 18-fold decrease in FAM84B as a hypothesis-generating screening observation that led to subsequent functional validation, rather than as evidence that intracellular tau accumulation itself directly suppresses FAM84B expression.

In the current study, FAM84B promoted the extracellular release of both wild-type and P301L-mutant 2N4R tau, with effects observed for the total and phosphorylated tau forms examined (Fig. 1 and Supplementary Fig. 5). Our findings support an association of FAM84B and tau within vesicle- or lipid-containing complexes rather than a stable detergent-resistant direct interaction (Fig. 2 and Supplementary Fig. 8). Accordingly, the apparent high-molecular-weight tau species is more consistent with tau co-migrating within a detergent-sensitive vesicle- or lipid-associated complex under detergent-free conditions than with a stable covalent tau–tau aggregate. FAM84B-associated tau redistribution was observed across the phosphorylation states examined, including T181, T231, S262, and S396/S404 (Supplementary Fig. 5F, G), indicating that, among the sites tested, this effect was not restricted to a single phosphorylation state. The co-fractionation of FAM84B and tau with EV-enriched preparations supports a potential role for FAM84B in vesicle-associated tau trafficking. Together with the gain- and loss-of-function results, these findings support redistribution of tau toward extracellular release, with an EV-associated component, rather than a simple reduction in intracellular tau burden. The association of FAM84B with vesicle- or lipid-containing extracellular compartments may be influenced by its structural and membrane-associated properties [35, 36]; however, the present data do not establish that FAM84B directly regulates EV biogenesis.

FAM84B, also known as LRATD2, contains an LRAT-homologous domain that shares sequence similarity with the H-Ras-like suppressor (HRASLS) family [37]. HRASLS proteins possess phospholipase A1/2 and acyltransferase activities involved in phospholipid metabolism [38], raising the possibility that the LRAT-like domain of FAM84B may contribute to its association with lipid membranes or membrane organization. Notably, however, FAM84B lacks the conserved catalytic cysteine required for the established phospholipase/acyltransferase activities of HRASLS proteins, and direct lipid-modifying enzymatic activity of FAM84B has not been established

[37]. Because we did not directly examine whether the LRAT-like domain or any lipid-modifying activity is required for EV-associated tau export, future studies using domain-specific mutants and lipidomic analyses will be needed to define this mechanism.

In additional cargo comparisons, FAM84B increased α-synuclein release into conditioned medium, whereas extracellular Aβ42 levels were unchanged; intracellular GFP levels were also not significantly altered (Supplementary Fig. 14A–E). These observations indicate that the effects of FAM84B are not uniform across the proteins examined and raise the possibility that FAM84B may preferentially facilitate the export of certain aggregation-prone or proteostasis-vulnerable proteins. Broader analyses of additional disease-associated proteins will be required to define the molecular features that distinguish permissive from non-permissive cargos and determine whether this selectivity depends on EV-associated packaging, the membrane-associated properties of FAM84B, or distinct cellular stress conditions.

Our pharmacological and genetic perturbation experiments collectively support contributions from RYR3-linked calcium signaling and clathrin-associated uptake to FAM84B-associated tau transfer (Figs. 3 and 4; Supplementary Fig. 11). The stronger effects of dantrolene and Pitstop2 relative to the corresponding siRNAs may reflect the broader pharmacological actions of these compounds, including inhibition of multiple ryanodine receptor isoforms or additional endocytic pathways, whereas the genetic experiments selectively perturbed individual components. Thus, our findings support RYR3 and CHC as contributing components of FAM84B-associated tau transfer but do not establish either pathway as an exclusive or obligate mediator. The contribution of CHC observed in our experiments is consistent with previous studies implicating clathrin-mediated endocytosis (CME) in extracellular tau uptake [39]. For example, LRP1 has been identified as an important mediator of tau internalization, and LRP1 depletion markedly reduces tau uptake and spread in experimental models [17]. However, our CHC knockdown and the broader effects of Pitstop2 indicate that clathrin-associated uptake should be considered one component of FAM84B-associated tau transfer rather than an exclusive internalization route.

Mounting evidence suggests that the pathogenesis of AD is not restricted to the neuronal compartment, but instead includes strong interactions with immunological mechanisms in the brain. Misfolded aggregates of Aβ are thought to bind to microglia and astroglia, triggering microglial activation and leading to the release of inflammatory cytokines such as IL-6 and TNF-α that contribute to disease progression as well as severity [40, 41]. Increased STAT3 Y705 phosphorylation and FAM84B levels were observed across several tauopathy groups (Figs. 1A and 5C). In line with these results, IL-6 increased FAM84B expression through STAT3-associated signaling (Fig. 5E, F), and TNF-α was also associated with increased FAM84B levels (Supplementary Fig. 12C). It should be noted that, although astrocytes and microglia are major participants in neuroinflammatory signaling in vivo [41], our cytokine experiments modeled the direct response of neuronal or neuron-like cells to inflammatory stimuli.

Several limitations should be considered when interpreting these findings. The human postmortem cohort was limited by demographic and neuropathological heterogeneity. The diagnostic groups were not age-matched, and the small and uneven numbers of male and female donors precluded reliable age-adjusted or sex-stratified analyses. Moreover, tissues were obtained from either the entorhinal cortex or middle temporal gyrus, and the sampled regions were not matched across diagnostic groups. Therefore, potential contributions of age, sex, cortical region, PMI, APOE genotype, neuropathological stage, and co-pathologies to the observed FAM84B, CHC, and phosphorylated STAT3 levels cannot be excluded. The available AD donors also had established neuropathological disease (Braak stages IV–VI), and subcortical and motor-related regions prominently affected in PSP and CBD were not examined; thus, the present data do not establish whether FAM84B upregulation occurs early in disease or precedes pathological tau spread. The CSF analysis was similarly exploratory, with only three participants per group and no statistically significant difference in FAM84B immunoreactivity. Future studies using larger CSF cohorts with validated quantitative assays and region- and stage-matched postmortem tissues will be required to address these limitations.

Several aspects of tau and model specificity also remain unresolved. Our mechanistic experiments primarily employed wild-type and P301L mutant 2N4R tau and therefore do not establish whether FAM84B-associated

export operates similarly across 3R, 4R, and mixed 3R+4R tau isoform backgrounds. In addition, although the high-molecular-weight tau signal observed under detergent-free conditions resolved to an apparent monomeric species after reducing treatment, the native conformational state of secreted or transferred tau was not determined; thus, preferential effects on soluble, oligomeric, or fibrillar tau cannot be inferred. The mechanistic studies were performed predominantly in HEK293, SH-SY5Y, and iPSC-derived cortical neuronal systems, and the FAM84B–STAT3–RYR3 pathway was not directly examined in purified astrocytes or microglia. Furthermore, the iPSC experiments used pooled samples generated from two genetically distinct lines per diagnostic group, providing group-level observations but preventing assessment of quantitative consistency across individual lines or clear separation of AD-associated effects from line-specific genetic-background effects. Future studies using isoform- and conformation-defined tau preparations, cell-type-specific neuronal and glial models, and larger panels of genetically diverse or isogenic iPSC lines will be needed to define the generalizability of this pathway.

The extracellular fractionation experiments also have technical limitations. Although the isolated fractions were enriched for the EV-associated markers Alix, TSG101, CD9, CD63, and CD81 and markedly depleted of calnexin (Fig. 2A), particle-size and morphological characterization and density-based separation were not performed. Accordingly, these preparations are interpreted as EV-enriched rather than EV-specific, and our findings support an EV-associated component of extracellular tau release rather than definitively demonstrating EV-specific tau transfer. Further orthogonal characterization consistent with MISEV guidelines will be required to define the extracellular vesicle populations involved [42].

Finally, the biological consequence of FAM84B-mediated tau transfer remains unresolved. We did not determine whether transferred tau induces pathological seeding or aggregate amplification, recipient-cell dysfunction or toxicity, or progressive tau pathology in vivo. Thus, the present findings do not establish FAM84B as a direct driver of tauopathy progression or determine the net biological consequence of increased intercellular tau transfer accompanied by reduced intracellular tau burden in donor cells. Instead, our results support neuroinflammatory cytokine signaling as an upstream regulator of a FAM84B-associated tau export-and-transfer program. Determining whether this process contributes to tauopathy progression in vivo and where it lies temporally within human disease progression will require further investigation.

Supplementary Information The online version contains supplementary material available at https://doi.org/10.1186/s12974-026-04069-7.

Acknowledgements We thank Dr. Peter Davies (Albert Einstein College of Medicine, USA), and Dr. J.E. Darnell, Jr. (Rockefeller University) for providing the materials (antibodies and plasmids) for this study. We thank Dr. Tiago Outerio for providing the materials (VN-Tau (P301L), Addgene plasmid #87634; Tau (P301L)-VC, Addgene plasmid #87633) for this study. The brain tissue and clinical data utilized for this study were provided by the Seoul National University Hospital (SNUH) Brain Bank and the SNUH Institution of Corpse-derived substance supply (SNUHBB 2023-05). We would also like to thank Pusan National University Hospital Brain Bank (PNUHBB; 2023-ER1002-01) for providing the samples of postmortem brain tissue and cerebrospinal fluid, and clinical data for this study.

Institutional review board statement This study was approved by the Institutional Review Board of the Korea Disease Control and Prevention Agency (reference number: 2022-07-06-2C-A).

Authors' contributions G.Y. and C.J. conceptualized the study. G.Y. and H.P. curated the data. G.Y., H.P., J.Y.P., J.Y.C., and M.K.K. performed formal analysis. C.J. and H.K. acquired funding. G.Y., H.P., M.K.K., J.H.K., and C.J. conducted the investigation. G.Y. and H.P. developed the methodology. C.J., H.K., and J.H.K. administered the project. S.H.P. and E.J.K. provided resources. C.J. supervised the study. G.Y., H.P., J.Y.P., M.K.K., and J.Y.C. performed validation. G.Y., H.P., and C.J. wrote the original draft. G.V.W.J., H.K., J.H.K., and Y.H.K. reviewed and edited the manuscript. All authors read and approved the final manuscript.

Funding The research received funding from grants (Jo C, 2022-NG-008-02 & 2025-NI-005-01; Kim H, 2023-NS-001-00) provided by the Korea Disease Control and Prevention Agency.

Data availability Data supporting the findings of this study can be obtained from the corresponding author upon request.

Declarations

Consent for publication All subjects who participated in the study provided their informed consent.

Competing interest The authors declare no competing interests.

Open Access This article is licensed under a Creative Commons Attribution-NonCommercial-NoDerivatives 4.0 International License, which permits any non-commercial use, sharing, distribution and reproduction in any medium or format, as long as you give appropriate credit to the original author(s) and the source, provide a link to the Creative Commons licence, and indicate if you modified the licensed material. You do not have permission under this licence to share adapted material derived from this article or parts of it. The images or other third party material in this article are included in the article's Creative Commons licence, unless indicated otherwise in a credit line to the material. If material is not included in the article's Creative Commons licence and your intended use is not permitted by statutory regulation or exceeds the permitted use, you will need to obtain permission directly from the copyright holder. To view a copy of this licence, visit http://creativecommons.org/licenses/by-nc-nd/4.0/.

References

1. Ritchie CW, Terrera GM, Quinn TJ. Dementia trials and dementia tribulations: methodological and analytical challenges in dementia research. Alzheimers Res Ther. 2015;7:31.
2. Giacobini E, Gold G. Alzheimer disease therapy–moving from amyloid-beta to tau. Nat Rev Neurol. 2013;9:677–86.
3. Haass C, Selkoe D. If amyloid drives Alzheimer disease, why have anti-amyloid therapies not yet slowed cognitive decline? PLoS Biol. 2022;20:e3001694.
4. Reitz C, Pericak-Vance MA, Foroud T, Mayeux R. A global view of the genetic basis of Alzheimer disease. Nat Rev Neurol. 2023;19:261–77.
5. Zhang Y, Wu KM, Yang L, Dong Q, Yu JT. Tauopathies: new perspectives and challenges. Mol Neurodegener. 2022;17:28.
6. Twohig D, Nielsen HM. α-synuclein in the pathophysiology of Alzheimer's disease. Mol Neurodegener. 2019;14:23.
7. Chung DC, Roemer S, Petrucelli L, Dickson DW. Cellular and pathological heterogeneity of primary tauopathies. Mol Neurodegener. 2021;16:57.
8. Crary JF, Trojanowski JQ, Schneider JA, Abisambra JF, Abner EL, Alafuzoff I, et al. Primary age-related tauopathy (PART): a common pathology associated with human aging. Acta Neuropathol. 2014;128:755–66.
9. Kalaria RN. The pathology and pathophysiology of vascular dementia. Neuropharmacology. 2018;134:226–39.
10. Chui HC, Ramirez-Gomez L. Clinical and imaging features of mixed Alzheimer and vascular pathologies. Alzheimers Res Ther. 2015;7:21.
11. Cummings JL, Gonzalez MI, Pritchard MC, May PC, Toledo-Sherman LM, Harris GA. The therapeutic landscape of tauopathies: challenges and prospects. Alzheimers Res Ther. 2023;15:168.
12. Chen Y, Yu Y. Tau and neuroinflammation in Alzheimer's disease: interplay mechanisms and clinical translation. J Neuroinflammation. 2023;20:165.
13. Cao J, Hou J, Ping J, Cai D. Advances in developing novel therapeutic strategies for Alzheimer's disease. Mol Neurodegener. 2018;13:64.
14. Kapoor M, Chinnathambi S. TGF-beta1 signalling in Alzheimer's pathology and cytoskeletal reorganization: a specialized tau perspective. J Neuroinflammation. 2023;20:72.
15. Mueller RL, Combs B, Alhadidy MM, Brady ST, Morfini GA, Kanaan NM. Tau: a signaling hub protein. Front Mol Neurosci. 2021;14:647054.
16. Wei Y, Liu M, Wang D. The propagation mechanisms of extracellular tau in Alzheimer's disease. J Neurol. 2022;269:1164–81.
17. Wu JW, Hussaini SA, Bastille IM, Rodriguez GA, Mrejeru A, Rilett K, et al. Neuronal activity enhances tau propagation and tau pathology in vivo. Nat Neurosci. 2016;19:1085–92.
18. Asai H, Ikezu S, Tsunoda S, Medalla M, Luebke J, Haydar T, et al. Depletion of microglia and inhibition of exosome synthesis halt tau propagation. Nat Neurosci. 2015;18:1584–93.
19. Rauch JN, Luna G, Guzman E, Audouard M, Challis C, Sibih YE, et al. LRP1 is a master regulator of tau uptake and spread. Nature. 2020;580:381–5.
20. van der Kant R, Goldstein LSB, Ossenkoppele R. Amyloid-beta-independent regulators of tau pathology in Alzheimer disease. Nat Rev Neurosci. 2020;21:21–35.
21. Ljubenkov PA, Rabinovici GD. Silencing tau to treat early Alzheimer's disease. Nat Med. 2023;29:1320–1.
22. Ransohoff RM. How neuroinflammation contributes to neurodegeneration. Science. 2016;353:777–83.

23. Uhm KO, Kim SJ, Jo EH, Go GY, Choi HY, Im YS, et al. Generation of human induced pluripotent stem cell lines from human dermal fibroblasts using a non-integration system. Stem Cell Res. 2017;21:13–5.
24. Im SY, Yoo DH, Kim HE, Oh JY, Kim YO. Generation of integration-free induced pluripotent stem cell line (KSCBi017-A) from peripheral blood mononuclear cells of a healthy male individual. Stem Cell Res. 2022;65:102965.
25. Pasca AM, Sloan SA, Clarke LE, Tian Y, Makinson CD, Huber N, et al. Functional cortical neurons and astrocytes from human pluripotent stem cells in 3D culture. Nat Methods. 2015;12:671–8.
26. Sonnleitner A, Conti A, Bertocchini F, Schindler H, Sorrentino V. Functional properties of the ryanodine receptor type 3 (RyR3) Ca2+ release channel. EMBO J. 1998;17:2790–8.
27. Becherer U, Moser T, Stuhmer W, Oheim M. Calcium regulates exocytosis at the level of single vesicles. Nat Neurosci. 2003;6:846–53.
28. Hunter CA, Jones SA. IL-6 as a keystone cytokine in health and disease. Nat Immunol. 2015;16:448–57.
29. Arriagada PV, Growdon JH, Hedley-Whyte ET, Hyman BT. Neurofibrillary tangles but not senile plaques parallel duration and severity of Alzheimer's disease. Neurology. 1992;42:631–9.
30. Xia C, Makeretz SJ, Caso C, McGinnis S, Gomperts SN, Sepulcre J, et al. Association of in vivo [18F]AV-1451 tau PET imaging results with cortical atrophy and symptoms in typical and atypical Alzheimer disease. JAMA Neurol. 2017;74:427–36.
31. Braak H, Braak E. Neuropathological stageing of Alzheimer-related changes. Acta Neuropathol. 1991;82:239–59.
32. Ising C, Venegas C, Zhang S, Scheiblich H, Schmidt SV, Vieira-Saecker A, et al. NLRP3 inflammasome activation drives tau pathology. Nature. 2019;575:669–73.
33. Heneka MT, Kummer MP, Stutz A, Delekate A, Schwartz S, Vieira-Saecker A, et al. NLRP3 is activated in Alzheimer's disease and contributes to pathology in APP/PS1 mice. Nature. 2013;493:674–8.
34. Maphis N, Xu G, Kokiko-Cochran ON, Jiang S, Cardona A, Ransohoff RM, et al. Reactive microglia drive tau pathology and contribute to the spreading of pathological tau in the brain. Brain. 2015;138:1738–55.
35. d'Errico P, Meyer-Luehmann M. Mechanisms of pathogenic tau and Abeta protein spreading in Alzheimer's disease. Front Aging Neurosci. 2020;12:265.
36. Huang Y, Yin H, Li B, Wu Q, Liu Y, Poljak K, et al. An in vitro vesicle formation assay reveals cargo clients and factors that mediate vesicular trafficking. Proc Natl Acad Sci U S A. 2021; 118.
37. Jiang Y, Lin X, Kapoor A, He L, Wei F, Gu Y, et al. FAM84B promotes prostate tumorigenesis through a network alteration. Ther Adv Med Oncol. 2019;11:1758835919846372.
38. Shinohara N, Uyama T, Jin XH, Tsuboi K, Tonai T, Houchi H, et al. Enzymological analysis of the tumor suppressor A-C1 reveals a novel group of phospholipid-metabolizing enzymes. J Lipid Res. 2011;52:1927–35.
39. Samudra N, Lane-Donovan C, VandeVrede L, Boxer AL. Tau pathology in neurodegenerative disease: disease mechanisms and therapeutic avenues. J Clin Invest. 2023;133.
40. Wyss-Coray T. Inflammation in Alzheimer disease: driving force, bystander or beneficial response? Nat Med. 2006;12:1005–15.
41. Heneka MT, Carson MJ, Khoury JE, Landreth GE, Brosseron F, Feinstein DL, et al. Neuroinflammation in Alzheimer's disease. Lancet Neurol. 2015;14:388–405.
42. Welsh JA, Goberdhan DCI, O'Driscoll L, Buzas EI, Blenkiron C, Bussolati B, et al. Minimal information for studies of extracellular vesicles (MISEV2023): From basic to advanced approaches. J Extracell Vesicles. 2024;13:e12404.

Publisher's Note Springer Nature remains neutral with regard to jurisdictional claims in published maps and institutional affiliations.

Authors and Affiliations

Gwangho Yoon[1,2] · Hyeyeon Park[3,4,5] · Jee-Yun Park[1] · Min Kyoung Kam[1] · Jung-Hyun Kim[3,4,6] · Eun-Joo Kim[7] · Sung-Hye Park[8] · Hyunyoung Kim[3,4] · Gail VW Johnson[9] · Ji-Young Choi[1] · Young Ho Koh[1] · Chulman Jo[1,2]

✉ Chulman Jo
chulmanjo@gmail.com

[1] Division of Brain Disease Research, Department for Chronic Disease Convergence Research, Korea National Institute of Health, 187 Osongsaengmyeong2-ro, Osong-eup, Cheongju-si, Chungcheongbuk-do 28159, Republic of Korea

[2] Division of Allergy and Respiratory Disease Research, Department for Chronic Disease Convergence Research, Korea National Institute of Health, 187 Osongsaengmyeong2-ro, Osong-eup, Cheongju-si, Chungcheongbuk-do 28159, Republic of Korea

[3] Division of Intractable Disease Research, Department for Chronic Disease Convergence Research, Korea National Institute of Health, 202 Osongsaengmyeong2-ro, Osong-eup, Cheongju-si, Chungcheongbuk-do 28160, Republic of Korea

[4] Korea National Stem Cell Bank, Korea National Institute of Health, 202 Osongsaengmyeong2-ro, Osong-eup, Cheongju-si, Chungcheongbuk-do 28160, Republic of Korea

[5] Adult Stem Cell Research Center and Research Institute for Veterinary Science, College of Veterinary Medicine, Seoul National University, Seoul 08826, Republic of Korea

[6] Department of Pharmacy, College of Pharmacy, Ajou University, 206 Worldcup-ro, Yeongtong-gu, Suwon-si 16499, Gyeonggi-do, Republic of Korea

[7] Department of Neurology, Pusan National University Hospital, Pusan National University School of Medicine and Biomedical research institute, Busan, Republic of Korea

[8] Department of Pathology, Seoul National University College of Medicine, Seoul 03080, Republic of Korea

[9] Department of Anesthesiology and Perioperative Medicine, University of Rochester, Rochester, NY, USA